



**THE MECHANICAL PROPERTIES AND MICROSTRUCTURE
ANALYSIS OF 308LSi AUSTENITIC STAINLESS STEEL
PRODUCED BY WIRE ARC ADDITIVE MANUFACTURING
(WAAM) TECHNIQUE**

MUHAMMAD NOR SAIFULLAIL BIN MOHD NOORAIMY

UNIVERSITI TEKNIKAL MALAYSIA MELAKA

B092010404

**BACHELOR OF MECHANICAL ENGINEERING TECHNOLOGY
(AUTOMOTIVE TECHNOLOGY) WITH HONOURS**

2024



Faculty of Mechanical Technology and Engineering

**THE MECHANICAL PROPERTIES AND MICROSTRUCTURE
ANALYSIS OF 308LSi AUSTENITIC STAINLESS STEEL
PRODUCED BY WIRE ARC ADDITIVE MANUFACTURING
(WAAM) TECHNIQUE**

Muhammad Nor Saifullail Bin Mohd Nooraimy

**Bachelor of Mechanical Engineering Technology (Automotive Technology) with
Honours**

2024

**THE MECHANICAL PROPERTIES AND MICROSTRUCTURE ANALYSIS OF
308LSi AUSTENITIC STAINLESS STEEL PRODUCED BY WIRE ARC
ADDITIVE MANUFACTURING (WAAM) TECHNIQUE**

MUHAMMAD NOR SAIFULLAIL BIN MOHD NOORAIMY

**A thesis submitted
in fulfilment of the requirements for the degree of
Bachelor of Mechanical Engineering Technology (Automotive Technology) with
Honours**



Faculty of Mechanical Technology and Engineering

UNIVERSITI TEKNIKAL MALAYSIA MELAKA

2024

BORANG PENGESAHAN STATUS LAPORAN PROJEK SARJANA MUDA

TAJUK: THE MECHANICAL PROPERTIES AND MICROSTRUCTURE ANALYSIS OF 308LSi AUSTENITIC STAINLESS STEEL PRODUCED BY WIRE ARC ADDITIVE MANUFACTURING (WAAM) TECHNIQUE.

SESI PENGAJIAN: 2023-2024 Semester 1

Saya **MUHAMMAD NOR SAIFULLAIL BIN MOHD NOORAIMY**

mengaku membenarkan tesis ini disimpan di Perpustakaan Universiti Teknikal Malaysia Melaka (UTeM) dengan syarat-syarat kegunaan seperti berikut:

1. Tesis adalah hak milik Universiti Teknikal Malaysia Melaka dan penulis.
2. Perpustakaan Universiti Teknikal Malaysia Melaka dibenarkan membuat salinan untuk tujuan pengajian sahaja dengan izin penulis.
3. Perpustakaan dibenarkan membuat salinan tesis ini sebagai bahan pertukaran antara institusi pengajian tinggi.
4. ****Sila tandakan (✓)**

☐

TERHAD

(Mengandungi maklumat yang berdarjah keselamatan atau kepentingan Malaysia sebagaimana yang termaktub dalam AKTA RAHSIA RASMI 1972)

☐

SULIT

(Mengandungi maklumat TERHAD yang telah ditentukan oleh organisasi/badan di mana penyelidikan dijalankan)

☒

TIDAK TERHAD



Disahkan oleh:



Alamat Tetap:

**JP& P, BLOK C1-06-01,
JLN PINANG, KEM SRI RUSA,
71050 PORT DICKSON, NEGERI SEMBILAN**

Cop Rasmi:

IR. TS. DR. LAULATUL HARINA BINTI PAJAN
Pensyarah Kanan
Jabatan Teknologi Industri
Fakulti Teknologi Kejuruteraan Mekanikal Dan
Pembuatan (FTKMP)
Universiti Teknikal Malaysia Melaka



Tarikh: 8 February 2024

Tarikh: 8 February 2024

**** Jika tesis ini SULIT atau TERHAD, sila lampirkan surat daripada pihak berkuasa/organisasi berkenaan dengan menyatakan sekali sebab dan tempoh laporan PSM ini perlu dikelaskan sebagai SULIT atau TERHAD.**

DECLARATION

I declare that this thesis entitled “ The Mechanical Properties and Microstructural Analysis of 308LSI Austenitic Stainless Steel Produced By Wire Arc Additive Manufacturing (WAAM) Technique ” is the result of my research except as cited in the references. The thesis has not been accepted for any degree and is not concurrently submitted in candidature of any other degree.

Signature :  

Name : Muhammad Nor Saifullail Bin Mohd Nooraimy

Date : 12/01/2024

.....

APPROVAL

I hereby declare that I have checked this thesis and in my opinion, this thesis is adequate in terms of scope and quality for the award of the Bachelor of Mechanical Engineering Technology (Automotive Technology) with Honours.

Signature

:



IR. TS. DR. LAILATUL HARINA BINTI PAIJAN
Penyarah Kanan
Jabatan Teknologi Industri
Fakulti Teknologi Kejuruteraan Mekanikal Dan
Pembinaan (FTKMP)
Universiti Teknikal Malaysia Melaka

Supervisor Name

: Ir. Ts. Dr. Lailatul Harina Binti Paijan

Date

: 12/01/2024

اونيورسيتي تيكنيكل مليسيا ملاك

UNIVERSITI TEKNIKAL MALAYSIA MELAKA

DEDICATION

I dedicate this final year paper to all those who played an important role in my academic journey, supported me throughout this endeavour, and inspired me to strive for excellence.

To my family who always love and encourage me my motivation. Your belief in my abilities and constant support have helped me become the person I am today. I will be forever grateful to you for your sacrifice and dedication to my studies.

To my friends, who have been my pillars of strength, always by my side during the challenges and triumphs of this academic pursuit. Your camaraderie, late-night study sessions, and endless discussions have made this journey enjoyable and memorable.

To my supervisors, who have imparted their knowledge and expertise, guiding me in my academic pursuits. Your passion for teaching, invaluable insights, and commitment to fostering intellectual growth have shaped my understanding and expanded my horizons.

To the countless researchers, scholars, and authors whose works have laid the foundation upon which this paper is built. Your dedication to advancing knowledge in your respective fields has been an inspiration and a guiding light throughout my research process.

Lastly, I dedicate this paper to myself, for the perseverance, determination, and countless hours poured into this project. It is a testament to my growth, resilience, and commitment to lifelong learning. May this serve as a stepping stone to a future filled with continued growth and exploration.

ABSTRACT

Wire arc additive manufacturing (WAAM) has emerged as a promising technology for manufacturing large and complex metal parts due to its high deposition rate and material versatility. 308LSi stainless steel is austenitic stainless steel known for its excellent corrosion resistance and good weldability. Understanding of the mechanical properties of 308LSi stainless steel is limited, especially about anisotropy. Therefore, the test samples were built using the CMT-WAAM robot system, parameters 115A, 11.6V and 4.0 m/min. Based on the tests performed, for tensile testing, specimens tested at 45° showed better results than specimens tested at 0° and 90°. This is due to the upward growth of columnar dendrites. Turning to the impact test, the average absorbed energy index was 65.03 J, 68.25 J, and 62.01 J for the 0°, 45°, and 90° samples, respectively. Notably, the 45° samples exhibited higher average energy absorption, indicating better impact resistance compared to the 0° and 90° samples. During the hardness test, average hardness values of 179.814 Hv, 167.66 Hv and 164.73 Hv were recorded for the lower, middle and top zones, respectively. The hardness value in the bottom zone exceeds the value in the upper zone. Finally, microstructural analysis shows that the dendrites grow following the built direction. The microstructure at the bottom zone is also finer than other zones because heat is conducted directly to the surface, so the cooling rate is higher. The microstructure of the middle zone is coarser than that of the bottom zone because as the residue increases, heat accumulates and the cooling rate is slower. The top zone is in direct contact with air and has a short time, so it is composed of equiaxed grains. According to the results test, it shows that the 308 LSi CMT-WAAM thin-wall has anisotropic mechanical behaviour.

اوينورسيتي تيكنيكل مليسيا ملاك

UNIVERSITI TEKNIKAL MALAYSIA MELAKA

ABSTRAK

Pembuatan aditif arka wayar (WAAM) telah muncul sebagai teknologi yang menjanjikan untuk mengeluarkan bahagian logam yang besar dan kompleks kerana kadar pemendapan yang tinggi dan serba boleh bahan. Keluli tahan karat 308LSi ialah keluli tahan karat austenit yang terkenal dengan rintangan kakisan yang sangat baik dan kebolehkimpalan yang baik. Pemahaman tentang sifat mekanikal keluli tahan karat 308LSi adalah terhad, terutamanya mengenai anisotropi. Oleh itu, sampel ujian dibina menggunakan sistem robot CMT-WAAM, parameter 115A, 11.6V dan 4.0 m/min. Berdasarkan ujian yang dilakukan, untuk ujian tegangan, spesimen yang diuji pada suhu 45° menunjukkan keputusan yang lebih baik berbanding spesimen yang diuji pada 0° dan 90°. Ini disebabkan oleh pertumbuhan dendrit kolumnar ke atas. Beralih kepada ujian impak, indeks tenaga serapan purata ialah 65.03 J, 68.25 J, dan 62.01 J untuk sampel 0°, 45° dan 90°, masing-masing. Terutamanya, sampel 45° mempamerkan purata penyerapan tenaga yang lebih tinggi, menunjukkan rintangan hentaman yang lebih baik berbanding sampel 0° dan 90°. Semasa ujian kekerasan, nilai kekerasan purata 179.814 Hv, 167.66 Hv dan 164.73 Hv masing-masing direkodkan untuk zon bawah, tengah dan atas. Nilai kekerasan di zon bawah melebihi nilai di zon atas. Akhir sekali, analisis mikrostruktur menunjukkan bahawa dendrit berkembang mengikut arah yang dibina. Struktur mikro di zon bawah juga lebih halus daripada zon lain kerana haba dialirkan terus ke permukaan, jadi kadar penyejukan lebih tinggi. Struktur mikro zon tengah lebih kasar daripada zon bawah kerana apabila sisa bertambah, haba terkumpul dan kadar penyejukan lebih perlahan. Zon atas bersentuhan langsung dengan udara dan mempunyai masa yang singkat, jadi ia terdiri daripada butir sama. Mengikut ujian keputusan, ia menunjukkan bahawa dinding nipis CMT-WAAM mempunyai tingkah laku mekanikal anisotropik.

UNIVERSITI TEKNIKAL MALAYSIA MELAKA

ACKNOWLEDGEMENTS

In the Name of Allah, the Most Gracious, the Most Merciful

First and foremost, I would like to thank and praise Allah the Almighty, my Creator, my Sustainer, for everything I received since the beginning of my life. I want to thank the Universiti Teknikal Malaysia Melaka (UTeM) for providing the research platform. Thank you also to the Malaysian Ministry of Higher Education (MOHE) for the financial assistance.

My utmost appreciation goes to my main supervisor, Ir. Ts. Dr. Lailatul Harina Binti Paijan, Faculty of Mechanical and Manufacturing Engineering Technology, Universiti Teknikal Malaysia Melaka (UTeM) for all her support, advice, and inspiration. Her constant patience in guiding and providing priceless insights will forever be remembered. Also, to my co-supervisor, Ts. Mohd Hairizal Bin Osman, Universiti Teknikal Malaysia Melaka (UTeM) who constantly supported my journey, and gave the help, and support I received from him.

Finally, from the bottom of my heart, I express gratitude to my beloved parents, Mohd Nooraimy Bin Musa and Nor Rizan Binti Abdul Malek, for his/her encouragement and who have been the pillar of strength in all my endeavours. My eternal love also to all my friends, Zarif Ikram, Raziqree, Zafran, Ariff Farhan, Nik Muhammad Mubasyir, Haqim, Nazmi and Rafiq for their patience and understanding. I would also like to thank my beloved siblings for their endless support, love, and prayers. Finally, thank you to all the individuals who provided me with the assistance, support, and inspiration to embark on my study.

TABLE OF CONTENTS

	PAGE
DECLARATION	
APPROVAL	
DEDICATION	
ABSTRACT	i
ABSTRAK	ii
ACKNOWLEDGEMENTS	ii
TABLE OF CONTENTS	iv
LIST OF TABLES	vi
LIST OF FIGURES	viii
LIST OF SYMBOLS AND ABBREVIATIONS	xiv
LIST OF APPENDICES	xv
CHAPTER 1 INTRODUCTION	16
1.1 Background	16
1.2 Problem Statement	17
1.3 Research Objective	18
1.4 Scope of Research	18
CHAPTER 2 LITERATURE REVIEW	19
2.1 Introduction	19
2.2 Additive Manufacturing Method	20
2.2.1 Laser Additive Manufacturing Process	20
2.2.2 Cold Spray Deposition Process	21
2.2.3 Laminated Object Manufacturing (LOM) Process	21
2.2.4 Wire Arc Additive Manufacturing	22
2.3 Wire Arc Additive Manufacturing (WAAM) Systems	22
2.3.1 Gas Tungsten Arc Welding (GTAW)	23
2.3.2 Plasma Arc Welding (PAW)	25
2.3.3 Gas Metal Arc Welding (GMAW)	25
2.3.4 Cold Metal Transfer (CMT)	27
2.4 Industrial Automation	29
2.5 Parameter for WAAM	31
2.6 Stainless steel	36
2.7 Mechanical Properties	37
2.7.1 Tensile Test	37

2.7.2	Impact Test	41
2.7.3	Hardness Test	42
2.8	Microstructure Analysis	45
2.9	Isotropy and Anisotropy	50
CHAPTER 3	METHODOLOGY	51
3.1	Introduction	51
3.2	Flow Chart	52
3.3	Materials	53
3.3.1	Stainless Steel 304 (Substrate)	53
3.3.2	Stainless Steel 308LSi (Filler wire)	53
3.4	Parameters	55
3.5	Experimental Setup	56
3.6	Equipment	60
3.6.1	ABB Robot Arm IRB (2600ID) and Welding Torch	61
3.6.2	Cold Metal Transfer Power Source	62
3.6.3	Robot Controller	62
3.6.4	Shielding Gas (Argon + O2)	63
3.7	Sample Preparation	64
3.7.1	Cutting Process	65
3.7.2	Milling Process	66
3.7.3	Electrical Discharge Machining (EDM)	68
3.7.4	Surface Grinding	72
3.8	Mechanical Properties	75
3.8.1	Tensile Test	75
3.8.2	Impact Test	80
3.8.3	Hardness Test	85
3.9	Microstructural Analysis	87
3.9.1	Optical Microscope	87
CHAPTER 4	RESULTS AND DISCUSSION	92
4.1	Introduction	92
4.2	Results and Analysis of Mechanical Properties and Microstructural Analysis	92
4.2.1	Tensile Test	92
4.2.2	Impact Test	97
4.2.3	Hardness Test	99
4.2.4	Microstructural Analysis	102
4.3	Summary	104
CHAPTER 5	CONCLUSION AND RECOMMENDATIONS	105
5.1	Conclusion	105
5.2	Recommendations	106
5.3	Project Potential	107
REFERENCES		108
APPENDICES		111

LIST OF TABLES

TABLE	TITLE	PAGE
Table 2.1	Process parameters during WAAM.	32
Table 2.2	CMT-WAAM optimised process parameters.	34
Table 2.3	Three levels of processing parameters.	35
Table 2.4	Tensile properties of WAAMed SS316L.	38
Table 3.1	Chemical Composition of SS308LSi filler wire.	55
Table 3.2	Mechanical Properties of SS308LSi filler wire	55
Table 3.3	Parameter of welding.	56
Table 3.4	Parameter for welding	56
Table 3.5	Parameter for hot mounting press	89
Table 4.1	Tensile test result for specimen 0°	93
Table 4.2	Tensile test result for specimen 45°	94
Table 4.3	Tensile test result for specimen 90°	95
Table 4.4	Average Values of the tensile test at different specimen angles (0°, 45°, 90°).	96
Table 4.5	Result of Charpy Impact Test for Specimen - 0°	97
Table 4.6	Result of Charpy Impact Test for Specimen - 45°	97
Table 4.7	Result of Charpy Impact Test for Specimen - 90°	98
Table 4.8	Data for Charpy Impact Test Energy Absorbed	98
Table 4.9	Result Hardness Value for Bottom Zone	99
Table 4.10	Result Hardness Value for the Middle Zone	100
Table 4.11	Result Hardness Value for Top Zone	100



LIST OF FIGURES

FIGURE	TITLE	PAGE
Figure 2.1	Schematic of WAAM systems (Xia et al., 2020)	23
Figure 2.2	Illustration of GTAW Torch. (Pan et al., 2018)	24
Figure 2.3	(a) Experimental setup of twin-wire WAAM system with preheating and trailing devices; (b) Schematic representation of the additive manufacturing process. (Pan et al., 2018)	24
Figure 2.4	Schematic diagram of the PAW-based WAAM system. (Pan et al., 2018).	25
Figure 2.5	Schematic of twin-wire welding torch for WAAM (Pan et al., 2018)	26
Figure 2.6	Schematic diagram of double electrode GMAW-based system. (Pan et al., 2018)	27
Figure 2.7	Cold Metal Transfer. (Selvi et al., 2018)	28
Figure 2.8	(I) Droplet deposition mechanism, (II) Arc ignition, (III) Immersion in the molten bath and arc quenching, (III) Retraction movement in short circuit, (IV) Inversion of movement. (Selvi et al., 2018)	28
Figure 2.9	Setup of WAAM system in a CNC gantry. (S. Singh et al., 2020)	30
Figure 2.10	Robotic arc setup of WAAM. (S. Singh et al., 2020)	30
Figure 2.11	Full appearance of a multilayer component by SpeedArc WAAM. (L. Wang et al., 2019)	33
Figure 2.12	Fabricated SS316L wall. (Senthil et al., 2023)	34
Figure 2.13	Stress-strain curves graph of SpeedPulse and SpeedArc tensile specimens along the horizontal direction. (L. Wang et al., 2019)	38

Figure 2.14 Stress-displacement curves for specimens of stainless steel and mild steel. (Haden et al., 2017)	39
Figure 2.15 Yield strength (Haden et al., 2017)	40
Figure 2.16 Ultimate tensile strength (Haden et al., 2017)	40
Figure 2.17 (a) Results of the tensile test specimen on L, T and D, (b) 0.2% proof stress, (c) ultimate tensile strength, (d) elongation. (Laghi et al., 2020)	41
Figure 2.18 Vicker hardness of specimens of the SpeedPulse and SpeedArc components. (L. Wang et al., 2019)	43
Figure 2.19 Hardness distribution along the build direction of the sample.(Senthil et al., 2023)	44
Figure 2.20 (a) grain growth orientation map and (b) austenite (γ) distribution map. (L. Wang et al., 2019)	46
Figure 2.21 (a) Optical micrographs along the transverse section of a specific layer of the component, (b) and (c) show higher magnification. (L. Wang et al., 2019)	46
Figure 2.22 Optical metallurgy graphs at the transverse cross-section of the components. (L. Wang et al., 2019)	47
Figure 2.23 Microstructure of the wall, (a) bottom region, (b) middle region and (c) top region.(Senthil et al., 2023)	48
Figure 2.24 Optical micrographs of the interfacial layer between weld lines (left) and repeating microstructural shifts observed near. (Senthil et al., 2023)	48
Figure 2.25 Optical micrographs of the interfacial layer between weld lines. (Laghi et al., 2020)	49
Figure 3.1 Flow chart	52

Figure 3.2 Stainless steel 304 (substrate)	53
Figure 3.3 SS308LSI (filler wire)	55
Figure 3.4 The shielding gas valve was switched on.	57
Figure 3.5 The Cold Metal Transfer (CMT) power supply was switched on.	57
Figure 3.6 The robot controller was switched on.	57
Figure 3.7 Clamp on the substrate to the table.	58
Figure 3.8 Parameter set on the CMT power source.	58
Figure 3.9 Deposition process.	59
Figure 3.10 Structure fabricated from CMT WAAM	60
Figure 3.11 Setup of equipment that is used in the WAAM process.	60
Figure 3.12 Robot arm and welding torch. IRB 2600ID	61
Figure 3.13 CMT power source. Fronius TPS 400i.	62
Figure 3.14 Robot Controller. IRC5 Controller.	63
Figure 3.15 Shielding Gas (Argon + O ₂)	64
Figure 3.16 Sample of WAAM.	64
Figure 3.17 Horizontal Bandsawing Machine PR-10V.	65
Figure 3.18 Cutting process (remove the substrate from the sample).	65
Figure 3.19 Sample after removing the substrate.	66
Figure 3.20 Vertical Turret Milling Machine. Model FM-15S	67
Figure 3.21 Milling process.	67
Figure 3.22 Sample before the milling process.	68
Figure 3.23 Figure 3.21 Sample after the milling process.	68
Figure 3.24 EDM Wire Cut Sodick VZ300	69
Figure 3.25 0.25mm diameter Brass EDM wire	69

Figure 3.26 Specimen arrangement in sample	70
Figure 3.27 Cutting Process	70
Figure 3.28 Samples after the cutting process.	71
Figure 3.29 Impact specimen at (0°)	71
Figure 3.30 Tensile Specimen at (0°)	71
Figure 3.31 Impact specimen at (45°)	71
Figure 3.32 Tensile specimen at (45°)	71
Figure 3.33 Impact specimen at (90°)	72
Figure 3.34 Tensile specimen at (90°)	72
Figure 3.35 Surface Grinder Proth PSGS-4080AHR	72
Figure 3.36 Specimen during the surface grinding process	73
Figure 3.37 Specimen before surface grinding	73
Figure 3.38 Specimen after surface grinding	74
Figure 3.39 Specimen of Impact Test before surface grinding process.	74
Figure 3.40 Specimen of Impact Test after surface grinding process	75
Figure 3.41 Dimension of the tensile specimen	76
Figure 3.42 Floor-Mounted Material Testing System. Instron Model 5585 Capacity 200KN.	77
Figure 3.43 Specimen of 0° before tensile test	77
Figure 3.44 Specimen of 0° after tensile test	78
Figure 3.45 Specimen of 45° before tensile test	78
Figure 3.46 Specimen of 45° after tensile test	79
Figure 3.47 Specimen of 90° before tensile test	79
Figure 3.48 Specimen of 90° before tensile test	80

Figure 3.49 ASTM E2	81
Figure 3.50 Universal Pendulum Charpy Impact Tester, 500 Joule	81
Figure 3.51 Specimen of 0° before impact test	82
Figure 3.52 Specimen of 0° after impact test	82
Figure 3.53 Specimen of 45° before impact test	83
Figure 3.54 Specimen of 45° after impact test	83
Figure 3.55 Specimen of 90° before impact test	84
Figure 3.56 Specimen of 90° after impact test	84
Figure 3.57 Vickers Hardness Tester. Shimadzu HMV-G31.	85
Figure 3.58 Cutting Sample Hardness from sample	86
Figure 3.59 Sample after the cutting process	86
Figure 3.60 Sample for Hardness Test	86
Figure 3.61 sample tested	87
Figure 3.62 Optical Microscope ZEISS AxioCam ERc 5s	88
Figure 3.63 Microstructure sample (90° aligned to build direction)	88
Figure 3.64 Cutting samples.	89
Figure 3.65 Mounting press machine Ecorpes 100	89
Figure 3.66 The specimens were encapsulated by using hot mounting presses. From left bottom, centre and top.	90
Figure 3.67 Grind process	90
Figure 3.68 Polish process	91
Figure 3.69 Etching process	91
Figure 3.70 Microstructure analysis	91
Figure 4.1 Graph for specimen 0°	93

Figure 4.2 Graph for specimen 45°	94
Figure 4.3 Graph for specimen 90°	95
Figure 4.4 Graph for Tensile stress at Maximum Load (MPa) at different angles of specimens	96
Figure 4.5 Graph of Average Energy Absorbed (J) at different angles of specimen	98
Figure 4.6 Graph for Average Hardness Value at different zones of specimens	101
Figure 4.7 Microstructures at the Bottom Zone	102
Figure 4.8 Microstructures at Middle Zone	102
Figure 4.9 Microstructure at Top Zone	103



LIST OF SYMBOLS AND ABBREVIATIONS

AM	-	Additive Manufacturing
WAAM	-	Wire Arc Additive Manufacturing
GMAW	-	Gas Metal Arc Welding
GTAW	-	Gas Tungsten Arc Welding
PAW	-	Plasma Arc Welding
CMT	-	Cold Metal Transfer
MIG	-	Metal Inert Gas
TIG	-	Tungsten Inert Gas
mm	-	millimetre



LIST OF APPENDICES

APPENDIX	TITLE	PAGE
APPENDIX A	Gant Chart PSM 1	111
APPENDIX B	Gant Chart PSM 2	112



CHAPTER 1

INTRODUCTION

1.1 Background

3D printing, another name for additive manufacturing, has advanced significantly in recent years. Technology can now produce intricate and valuable final products, surpassing the need for prototyping. (Pérez et al., 2020). Two factors driving the growth of additive manufacturing are the industry's versatility and ongoing technological advancements. Technology is developing as a result of consumer demand for customised goods, quicker cycles for product development, increased focus on sustainability, lower manufacturing costs and lead times, and creative business strategies. This technology is rapidly spreading across various industry sectors, including the aerospace, automotive and biomedical industries, with notable growth in the medical device and wearable markets. According to (Bikas et al., 2016), it still has the disadvantages of limited production, poor quality, and unclear mechanical quality.

Additive manufacturing has various types and techniques that are used for different purposes in different industries. Some of the types of additive manufacturing include ceramic-based additive manufacturing, which is used for printing bioceramics and functionally graded materials, polymer-based additive manufacturing, which involves printing with polymers and can include techniques such as fused deposition modeling (FDM) and stereolithography (SLA). According to (Li et al., 2019), metal additive manufacturing which involves printing with metals has four types Binder Jetting, Power Bed Fusion, Sheet Lamination and Direct Energy Deposition (DED). Each type of additive manufacturing has its advantages and applications, such as improved design flexibility, the ability to build porous structures, and on-demand production. The choice of additive manufacturing technique depends on the specific requirements of the application and the materials being used.

An essential method for creating three-dimensional metal structures is wire arc additive manufacturing or WAAM. To cut expenses and time, it is being used more and more frequently worldwide. Four heat sources are utilised in WAAM: cold metal transfer (CMT), plasma arc welding (PAW), tungsten inert gas welding (TIG), and metal inert gas welding (MIG). MIG is easier and more convenient than TIG and PAW because it uses a continuous coil with the welding torch. TIG and PAW welding, in contrast to MIG, need an external wire feed mechanism to supply extra material. (Le et al., 2021). Cold metal transfer, an improved form of inert gas (MIG) welding, has a more stable arc than traditional MIG. CMT also reduces heat input, resulting in lower residual stresses and strains. Among these technologies, CMT is a great fit for WAAM.

1.2 Problem Statement

Additive manufacturing (AM), commonly known as 3D printing or rapid prototyping, is a revolutionary process that builds objects layer by layer using 3D model data. Unlike subtractive manufacturing methods, AM excels in its ability to create complex designs with high digitization and geometric freedom. This technique minimizes material usage and waste, thus promoting the sustainability of production. According to (Dinovitzer et al., 2019), wire arc additive manufacturing (WAAM), which uses a welding arc as the primary heat source, is increasingly recognized for its superior properties, including rapid deposition High deposition and optimal material utilization efficiency. This innovative technique involves layer-by-layer fusion and deposition of metal wire to fabricate parts, providing significant benefits in efficiency and resource utilization.

Although Wire Arc Additive Manufacturing (WAAM) has drawn a lot of interest in producing parts made of titanium and aluminium alloys, particularly for the aerospace and military sectors (Wu et al., 2018), the use of low-carbon and austenitic stainless steels has been central to the WAAM exploration of steel component production. Previous studies, such as that of (Hadjipantelis et al., 2022), showed anisotropy in the mechanical response of WAAM stainless steel, suggesting that its behaviour is influenced by certain factors. Similar to (C. Wang et al., 2022), who conducted a comparative study on 316 stainless steel parts produced by WAAM, highlighting the anisotropy of microstructure and mechanical properties.

308LSi, austenitic stainless steel, finds widespread use in gas, oil, mining, and automotive industries due to its lower carbon content. This study is dedicated to investigating the mechanical properties, and microstructure of thin-walled 308L components fabricated through the CMT-WAAM process and identifying if there is anisotropy behaviour on the components.

1.3 Research Objective

The main aim of this research is to evaluate the austenitic stainless steel (308LSi) structure manufactured with a 3D printed structure using a robotic melting process. Specifically, the objectives are as follows:

- a) To develop and fabricate the CMT-WAAM structure using robotic welding.
- b) To study the mechanical properties of the CMT-WAAM structure.
- c) To analyse the microstructure of the CMT-WAAM structure.

1.4 Scope of Research

The scope of this research is as follows:

- Conducting experiments with the CMT power source will be employed for the WAAM fabrication process, utilizing robot welding.
- Mechanical Testing: To evaluate the mechanical properties of the fabricated austenitic stainless steel (308LSi) for tensile testing, hardness testing and impact testing.
- Microstructure Analysis: Examine the microstructure of the WAAM-fabricated austenitic stainless steel (308LSi) using Optical Microscopy (OM).

CHAPTER 2

LITERATURE REVIEW

2.1 Introduction

The potential of additive manufacturing, commonly referred to as 3D printing, to produce intricate geometries quickly and without assembly has drawn both commercial and public interest for over 30 years. The main reasons behind additive manufacturing's expansion are its capacity to work with a large range of materials and ongoing technological advancements. Technological development is aided by the need for customized products, quicker cycles for product development, increased focus on sustainability, lower production costs and delivery times, and creative business models. According to (Pérez et al., 2020) the three characteristics of a revolutionary idea universal, practical, and efficient are present in additive manufacturing, and as a result, traditional manufacturing starts to make way for these new technologies. Technology is swiftly advancing across various industrial sectors, including aeronautics, automotive, and biomedicine. There is notable progress, particularly in the fields of medical devices and wearables.

Within the context of Industry 4.0, additive manufacturing occupies a central role and is acknowledged as a crucial technology that will facilitate the fourth industrial revolution. To attain widespread industry implementation, it is essential to develop and test materials, prioritize the implementation of efficient procedures, and tackle design and software obstacles. Based on, (Ryalat et al., 2023), this approach is necessary to support the manufacturing of customised, superior products in extremely productive smart factories that exhibit smooth cyber-physical integration and are consistent with the ideas of the Industry 4.0 movement.

As an additive manufacturing technique, wire arc additive manufacturing (WAAM) builds physical objects by layer-by-layer addition of material. It is a type of directed energy deposition (DED) process in which wires are melted using an electric arc and then selectively

deposited to form the part. Since WAAM can satisfy the dimensional requirements of structural elements, the current focus is on developing processes for use in the construction industry to improve the efficiency of materials used in construction. Furthermore, by utilizing WAAM, design limitations imposed by traditional subtractive forming and manufacturing processes can be lifted, improving structural optimization. Several more metal constructions showed enhanced structural performance. (Evans et al., 2023) .

2.2 Additive Manufacturing Method

Additive manufacturing (AM) is a widely used technique that greatly enhances manufacturing capabilities and flexibility to produce parts with intricate shapes. Lately, additive manufacturing (AM) has enabled the production of dense parts with optimal quality from crucial engineering materials like titanium, steel, and aluminium. Lately, AM has shown to be a fantastic substitute for layer-by-layer construction of parts. AM techniques include wire arc additive manufacturing (WAAM), layered object manufacturing (LOM), cold spray deposition, and laser additive manufacturing.

Building structures in metal using Additive Manufacturing (AM) holds widespread applicability across diverse industries. Post-processing is an integral aspect of working with metal, crucial even in swift procedures like metal casting. This post-processing step serves to refine the structure, necessitating adjustments in resolution for enhanced production efficiency compared to conventional AM methods. The versatility of AM in metals extends to repair work, offering on-site solutions for repairing ships and other structures promptly. Simultaneously, it finds its niche in the creation of tailor-made metallic components and end-products, meeting the specific requirements of various industries. (Evjemo et al., 2022).

2.2.1 Laser Additive Manufacturing Process

Products with improved external and internal surfaces, precise shapes, and faster production times can be produced thanks to the laser additive manufacturing process. The ability to produce parts with consistent structural integrity is one of its advantages over other AM processes. Minimum distortion and substantial power savings are achieved by precise operation with low heat input. Moreover, wire-based and powder-based techniques are the

two varieties of laser additive manufacturing available. A wire-based method involves continuously melting the wire and introducing the powder into the molten zone of the surface that faces the laser, either by pre-deposition or continuous introduction. This technology's primary drawbacks are its slow material deposition, size restrictions, lengthy processing times, and increased manufacturing costs. (S. R. Singh & Khanna, 2021).

2.2.2 Cold Spray Deposition Process

The cold spray deposition process is a technique that uses the kinetic energy of the material while also requiring thermal energy to deposit the material. This method depends on the underlying plastic deformation of micron-sized particles (less than 100 mm) and the attachment of particles to the substrate through a combination of physical interlocking and fusion. metal to metal. The main characteristics of the cold spray technique include thermal phase transformation during deposition and reduced stress generation. The velocity of the incident powder particles must be maintained for effective deposition. However extreme caution must be exercised because the powder will lose its adhesion properties when the vibrations decrease below the critical speed. When the speed of the powder particle exceeds the threshold, erosion is almost inevitable. The entire cold spray deposition process depends on variables such as gas flow, particle size and speed. The impregnated layer in this method has almost no ductility and requires additional heat treatment. This procedure requires good visibility so the outer surface is easier to use than the inner surface.. (S. R. Singh & Khanna, 2021).

2.2.3 Laminated Object Manufacturing (LOM) Process

Using sheet metal as a raw material is known as LOM. Ultrasonic fusion (UC) and ultrasonic additive manufacturing (UAM) are commonly used to fuse a stack of precisely cut metal layers to create three-dimensional parts. To prevent melting, ultrasonic waves are used to pressurise the cell to a standard temperature and diffuse the surface. A heat source should not be used to fuse stacked panels into a three-dimensional object. Before UC bonding, the metal sheet is cut to the proper size and shape. Traditional methods of polishing the surface are used when detailed finishing is needed. The issue with this method is that

composting the leaves requires more time and work. Additionally, hollow and scalloped parts cannot be created using this method. (S. R. Singh & Khanna, 2021).

2.2.4 Wire Arc Additive Manufacturing

In the WAAM process, the arc acts as the heat source, and the coils are the raw material that is used to deposit three-dimensional objects. In 1920, this system was granted its first patent. It is more efficient than other additive manufacturing processes because it uses less material and has less expensive equipment. Based on the CAD model, molten metal droplets are continuously transferred to the surface. Compared to traditional AM techniques, WAAM offers the following benefits: 100% material utilisation, reduced costs, faster production rates, and improved layer combination in parts. The WAAM process yields a different structure than that produced conventionally, and it shortens the time required to produce large parts with less complexity. Despite this, the module's surface quality is not as good as it could be given conventional manufacturing techniques. While stability was necessary for the WAAM process, residual stresses, unclean surfaces, warping from overheating, and imprecise work leading to stair treads were significant issues. (S. R. Singh & Khanna, 2021).

2.3 Wire Arc Additive Manufacturing (WAAM) Systems

An electric arc is used as a heat source in wire arc additive manufacturing (WAAM), an emerging technology that deposits metal layer by layer, as the final part (Figure 2.1) illustrates. Generally, WAAM offers four types of welding depending on the heat source: cold metal transfer (CMT), gas tungsten arc welding (GTAW), gas metal arc welding (GMAW), and plasma arc welding (PAW). Since 1925, the process of depositing the complete piece of welded metal has been in use. (Xia et al., 2020).

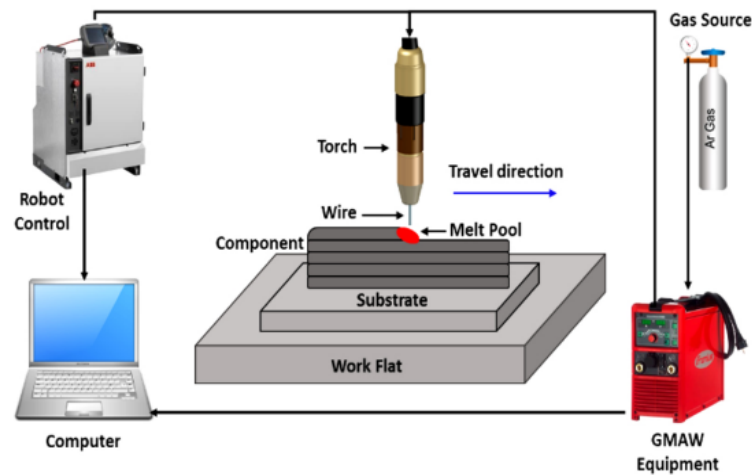


Figure 2.1 Schematic of WAAM systems (Xia et al., 2020)

2.3.1 Gas Tungsten Arc Welding (GTAW)

Based on (Pan et al., 2018) GTAW produces weld residue by using a separate power supply wire in conjunction with a non-consumable tungsten electrode, as illustrated in Figure 2.2. The quality of material transport and deposition is impacted by wire orientation during deposition. Rear, side, and front feeding are all available. Top-feeding is frequently employed with Ti- and Fe-based AM. A mathematical model to optimise the direction and location of wire feed was developed to improve the deposition process' accuracy. The lengthening of the arc causes a proportional increase in the distance between the workpiece and the protective nozzle. A laminar shielding gas flow is produced by a gas lens to lessen oxidation. When processing titanium alloys outside, anti-leakage devices are typically employed to stop the alloys from oxidising.

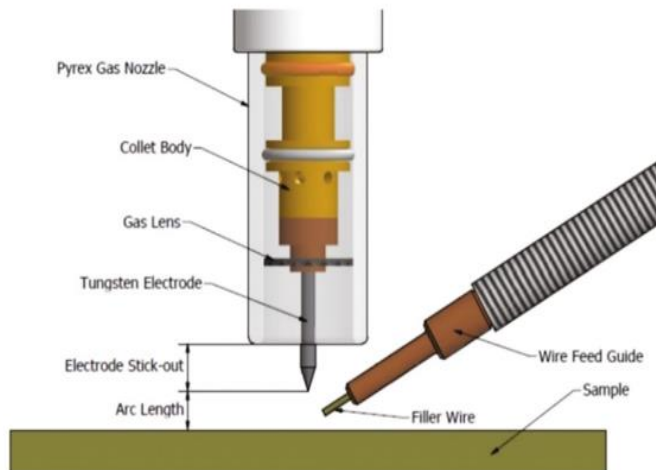


Figure 2.2 Illustration of GTAW Torch. (Pan et al., 2018)

To produce intermetallic materials, a two-wire WAAM based on GTAW was created and is categorised according to its function. Two different wires from a separate wire feed system are fed into a single weld pool to fabricate the objects. It is possible to modify the composition of various materials by altering the individual wire flow rates. It is possible to employ preheating and flue gas protection to control the temperature in between passes and stop oxidation. A two-wire experimental WAAM setup and a schematic diagram of the manufacturing process are shown in Figure 2.3.

UNIVERSITI TEKNIKAL MALAYSIA MELAKA

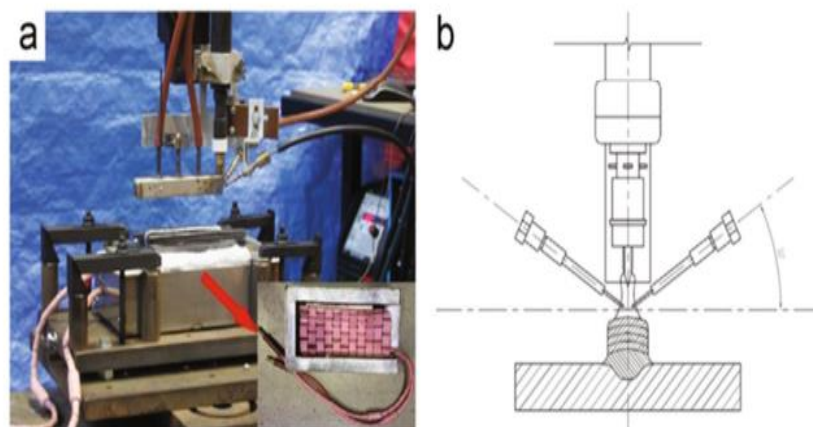


Figure 2.3 (a) Experimental setup of twin-wire WAAM system with preheating and trailing devices; (b) Schematic representation of the additive manufacturing process. (Pan et al., 2018)

2.3.2 Plasma Arc Welding (PAW)

A lot of research has also been done on plasma arc welding (PAW), an additive manufacturing technique for metallic materials. With an arc energy density of up to three times greater than GTAW, plasma welding produces smaller welds and less weld distortion at higher welding speeds. As seen in Figure 2.4, a published WAAM system is based on micro-PAW. (Pan et al., 2018).

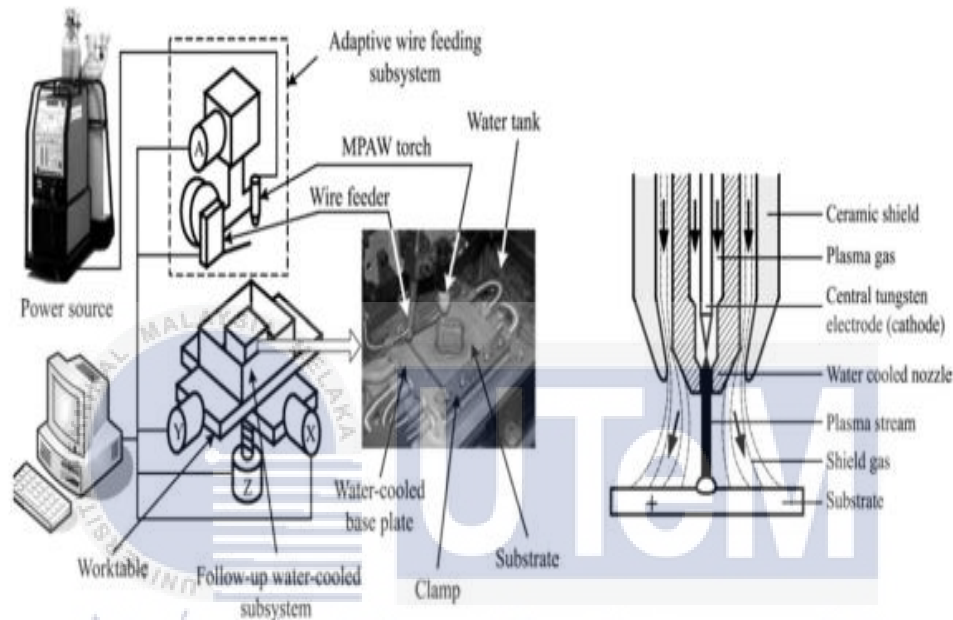


Figure 2.4 Schematic diagram of the PAW-based WAAM system. (Pan et al., 2018).

2.3.3 Gas Metal Arc Welding (GMAW)

An electric arc is created between a metal workpiece and a consumable wire electrode during the gas metal arc welding (GMAW) process. The wire usually lies parallel to the ground. Using the single-wire method, mobility during deposition is unaffected by the necessity to rotate the torch. In GMAW, injection and pulse injection are two examples of the different transfer mechanisms that can be used. WAAM has made extensive use of cold metal transfer (CMT), a modified GMAW variant based on controlled immersion transfer, because of its quick deposition rate and low heat input. (Pan et al., 2018).

According to a recent publication, the tandem GMAW two-wire process can produce metallic objects with high deposition rates, as shown in Figure 2.5. It has been stated that the tandem system can create gradient materials as well as intermetallic alloys.

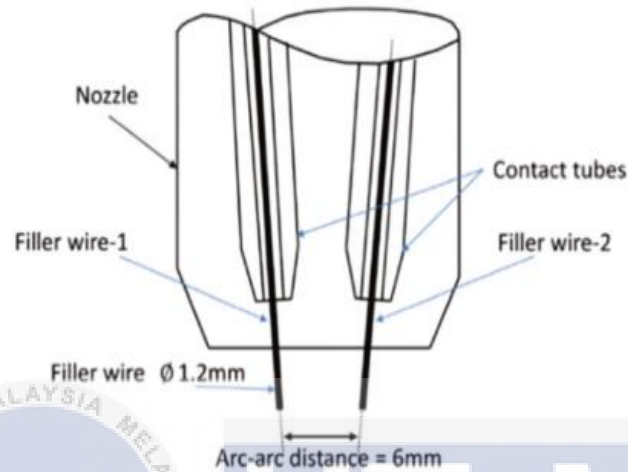


Figure 2.5 Schematic of twin-wire welding torch for WAAM (Pan et al., 2018)

As seen in Figure 2.6, a dual-electrode GMAW system that generates bypass current using a GTAW torch has been developed to improve material performance and deposition rates. The material utilisation factor rose by more than 10% when thin-walled parts were deposited using DE-GMAW within a particular bypass current range. Any wire arc system with multiple electrodes or conductors requires the torch to be aligned in the direction of travel, which adds a significant additional constraint to the path-planning process.

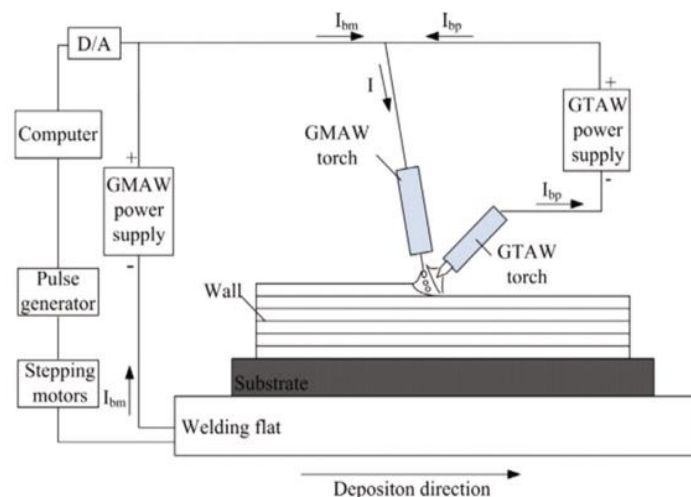


Figure 2.6 Schematic diagram of double electrode GMAW-based system. (Pan et al., 2018)

2.3.4 Cold Metal Transfer (CMT)

According to (Selvi et al., 2018), Fronius of Austria invented cold metal transfer welding (CMT), an enhanced MIG welding technique, in 2004. The mechanical drop-cutting method is the only way that this welding process varies from MIG and MAG welding processes. Temperature variations in the base metal and weld joint during the welding process have a big impact on the welded product's dimensional and shape accuracy, as well as its material properties and residual stresses. CMT welding uses a high-speed digital control system in conjunction with an innovative wire feed system to provide low heat input and controlled material deposition. To ensure that there is sufficient energy to melt both the base material and a drop of filler wire, the wire feed rate and arc phase of the cycle are controlled.

Based on GMAW, the CMT process is an improved version of the WAAM process. The CMT-WAAM system's fundamental parts are the robot, wire feed motor, welding apparatus, and computer controller. The method for separating metal droplets is the primary distinction between GMAW and CMT. The reason this process is called CMT is that it produces less heat than the traditional GTAW-WAAM method. Reduced heat input makes it possible to achieve low and regulated metal deposition rates. An arc forms at the metal feed wire's tip as it advances in the direction of the base (base plate). Arc amplification may happen as the wire approaches the weld pool. A short circuit in the system may happen the instant the power cord tip comes into contact with the solder pool. The power cord is raised to a specific height in the event of a short circuit. Water droplets detach from the wire tip and enter the weld pool as the wire moves backwards. There will be less heat produced in the weld pool as a result of the short circuit phenomenon that occurs during the deposition process. The primary benefit of this procedure is this. CNC has developed several advanced processes, such as CMT Pulse (CMT-P), CMT Advanced (CMT-ADV), and CMT Pulse Advanced (CMT-PADV). Figure 2.7 shows Cold Metal Transfer. (Selvi et al., 2018) Figure 2.8 indicates the mechanism of droplet deposition.

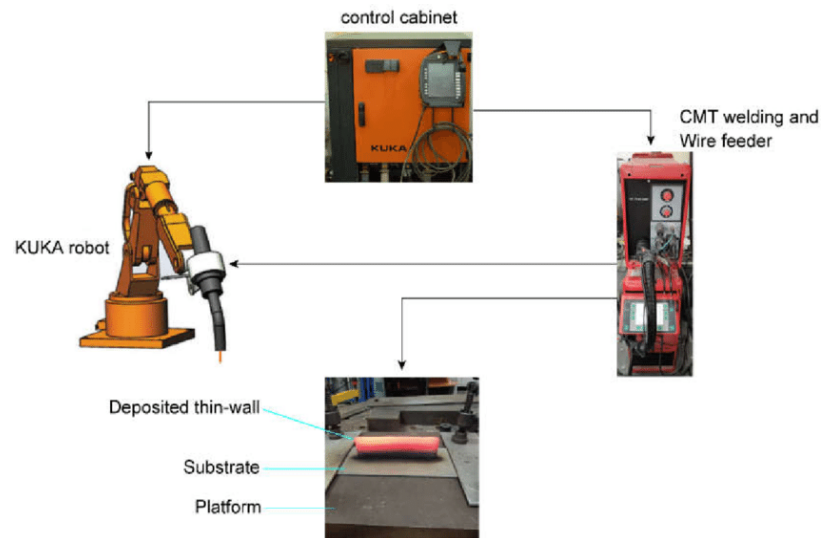


Figure 2.7 Cold Metal Transfer. (Selvi et al., 2018)

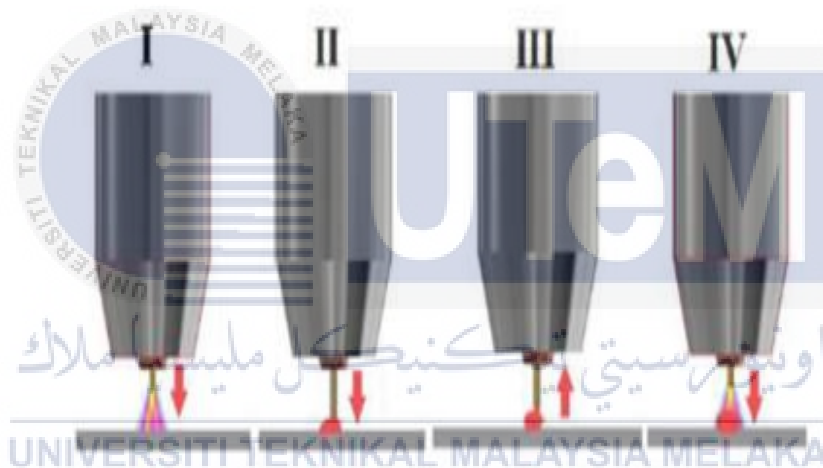


Figure 2.8 (I) Droplet deposition mechanism, (II) Arc ignition, (III) Immersion in the molten bath and arc quenching, (III) Retraction movement in short circuit, (IV) Inversion of movement. (Selvi et al., 2018)

Due to its simplicity of use, gas metal arc welding (GMAW), also referred to as metal inert gas (MIG) welding, seems to be the recommended technique for robotic wire arc additive manufacturing (WAAM). In contrast, an external supply of welding material is required for gas tungsten arc welding (GTAW), also known as tungsten inert gas (TIG) welding. Notably, the welding gun's nozzle, which serves as the electrode in MIG, is where the welding material is introduced. Due to this design, only the welding gun nozzle needs to be taken into consideration when determining the robot's end-effector path. On the other hand, TIG adds another external barrier to wire feeding, which makes MIG more streamlined and advantageous for effective WAAM procedures.(Evjemo et al., 2022).

Compared to conventional GMAW, cold metal transfer (CMT), an enhanced version of metal inert gas welding (GMAW), produces a more stable arc. Metal spatter, also known as "welding spatter," is significantly reduced as a result of this increased stability. Furthermore, CMT displays a lower heat input, which results in lower residual stress and distortion in the weld material. (Baoqiang et al., 2016). These distinctive properties make CMT particularly well-suited for Wire Arc Additive Manufacturing (WAAM), where precision, stability, and minimized distortions are crucial for successful layer-by-layer surfacing.

2.4 Industrial Automation

The traditional gantry system used in 3D printing and other 3-axis CNC machines is frequently used in wire arc additive manufacturing (WAAM). The fixed tool is swapped out for the welding torch, resulting in the full WAAM setup seen in Figure 2.9. Similar to the print bed's vertical movement, the welding torch's movement on the flat plane is constrained by a PC framework that is locally accessible.

According to (S. Singh et al., 2020), the constant vertical motion of the melt pool wire, which causes the wire to melt and bead deposition at the end of each layer, is one of the difficulties with these 3D structures. Simpler structures have an innate vibration that can cause the weld pool to become unstable. To address this, new computer programming and control procedures are put in place to manage the arc and guarantee a stable and regulated build-up of weld beads.

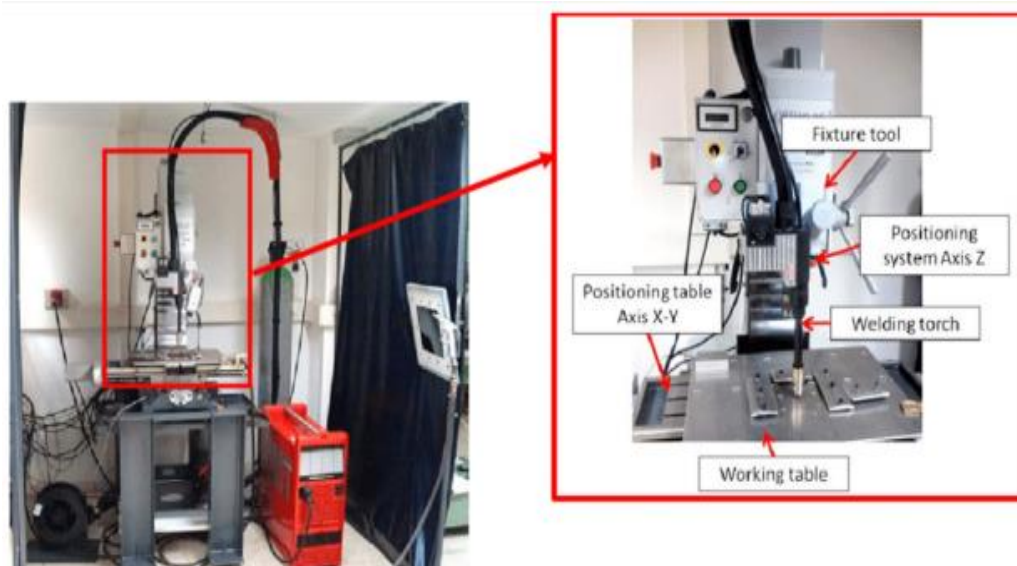


Figure 2.9 Setup of WAAM system in a CNC gantry. (S. Singh et al., 2020)

Experiments involving Wire Arc Additive Manufacturing (WAAM) are increasingly using robotic arm setups. Figure 2.10 shows the integration of robotic assistance with a cold metal transfer system for WAAM. A robotic wire feed system outperforms conventional gantry systems in WAAM setups. Robotic assistance significantly enhances weld bead deposition while reducing the stair-step effect. This improvement is ascribed to the robotic arm's ability to precisely and flexibly weld metal in all six directions.

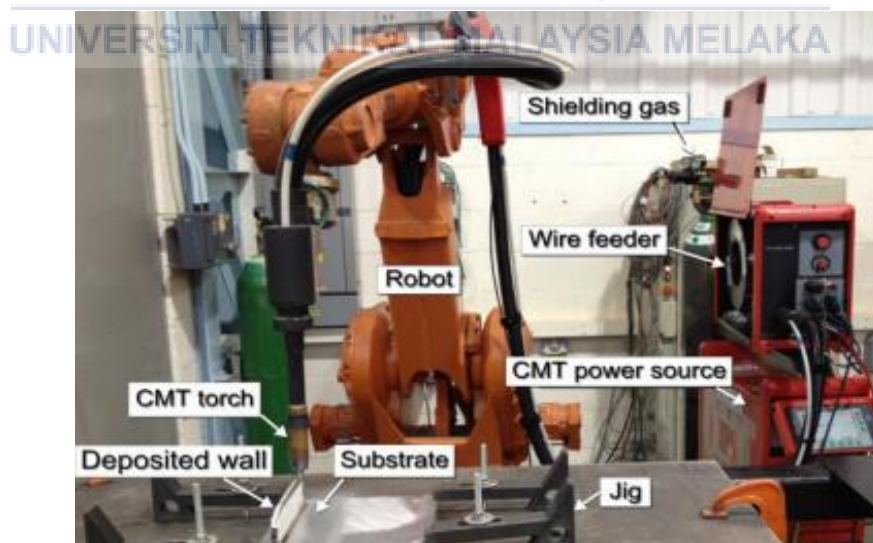


Figure 2.10 Robotic arc setup of WAAM. (S. Singh et al., 2020)

2.5 Parameter for WAAM

During the WAAM process, three important welding process variables need to be carefully chosen and kept an eye on. Wire feed speed, welding voltage, and welding current are these parameters. When combined, these variables will have an impact on the heat input during the welding process, which will have an impact on the weld's characteristics.

According to (S. Singh et al., 2020), the most important factor influencing the electrode burning rate, melting depth, and weld shape during the arc welding process is current. Wire feed speed is related to welding current. As the current increases, so does the weld penetration depth. The strength of the weld increases with depth.

The arc voltage is the potential difference that exists between the welding wire tip and the workpiece or weld pool. It establishes the fusion zone's state and the weld's strength. The ideal arc voltage is reached at the greatest penetration depth. (S. Singh et al., 2020).

Weld penetration and bead size are influenced by welding speed, also known as arc travel speed. As transit speed increased, metal deposition decreased. Consequently, to increase the deposition thickness, the movement speed must be decreased. Welding speed needs to be carefully adjusted based on the joint structure and thickness of the material. (S. Singh et al., 2020).

The distance from the contact tip to the end tip of the wire, where the arc originates, is called the wire extension. Stretching can result in too much weld bead, poor shape, and insufficient penetration. In general, the extended length of the wire is kept as constant as possible. (S. Singh et al., 2020).

Based on the experiment of (L. Wang et al., 2019) a commercial grade 316L stainless steel sheet with dimensions of 250 x 100 x 5 mm³ was selected as the substrate, and components were positioned using 1.2 mm diameter 316L stainless steel wire. Arc auxiliary manufacturing tests can be carried out with two distinct arc modes by utilising a FANUC 6-axis robot integrated with a Lorch power source. SpeedPulse and SpeedArc are two common arc mode types provided by Lorch Schweißtechnik GmbH. The modified I-I-I controlled, short-circuit-free pulse welding process used in SpeedPulse mode operates at a constant

frequency and combines the features of a pulsed arc to achieve high process reliability, typically with the characteristics of the classic spray arc. The main metal transfer mode in SpeedPulse WAAM is the spray transfer mode. Excellent directional stability and high power density are delivered by SpeedArc WAAM, which differs from conventional GMAW with its short, incredibly powerful arc in the spray arc range. The primary metal transfer mode in SpeedArc WAAM is the short circuit transfer mode. We used 99.99% pure argon as a protective gas. The length of a single layer is 150 mm. Because the scanning path has been scanned back and forth, the scanning direction in the current layer is opposite to the scanning direction in the previous layer. For twenty seconds, the change to the next nearby floor is halted. Figure 2.11 displays the sample test, and Figure 2.10 displays the process parameters.

Table 2.1 Process parameters during WAAM.

Arc mode	SpeedPulse WAAM	SpeedArc WAAM
Mean current I /A	22.1	19.5
Mean voltage U /V	135	140
Arc power P /W	2984	2730
Layer n	30	30
Scanning speed v_1 /(mm s ⁻¹)	10	10
Wire feeding rate v_2 /(m min ⁻¹)	4.5	4.5
Gas flow rate Q /(L min ⁻¹)	25	25
Layer thickness δ /(mm)	1.5	1.8

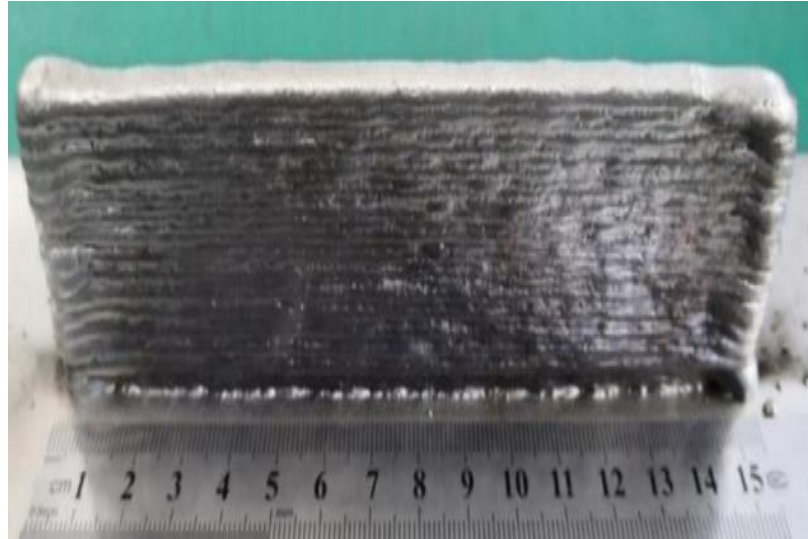


Figure 2.11 Full appearance of a multilayer component by SpeedArc WAAM. (L. Wang et al., 2019)



As demonstrated by (Senthil et al., 2023), A single wall was built as a demonstration of the capabilities of the CMT-based WAAM (Wire Arc Additive Manufacturing) process (Figure 2.10). The wall measures 70 mm in height, 120 mm in width, and 16 mm in thickness. This is accomplished by depositing twenty 3.5 mm high SS316L layers onto a 14 mm thick SS316L substrate. Reciprocal deposition is the method employed. During the CMT process, molten metal is deposited with a very low heat input during wall construction. Fans and aluminium fins have been positioned beneath the substrate to enhance cooling. An entirely automated and continuous wall construction process is ensured by the use of CMT robots. Crucially, there are no interruptions or pauses between layers as a result of this automation. Table 2.2 contains the parameters.



Figure 2.12 Fabricated SS316L wall. (Senthil et al., 2023)

Table 2.2 CMT-WAAM optimised process parameters.

Material Deposited	Deposition Current (A)	Wire feed rate (mm/min)	Travel speed (mm/min)
Inconel 825	146	5000	150
SS316L	113	3800	150

Based on the study of (Le & Mai, 2020), Using 1mm diameter GM-308L commercial stainless steel wire (provided by Kim Tin Viet Company), thin-walled samples are created on 200mm x 100mm x 10mm SS400 steel plate using a GMAW commercial robot (Panasonic TA1400). Nam supplied). To examine the microhardness and microstructure of the material that was fabricated, a thin-walled sample measuring 20 mm in height and 100 mm in length was first created. A second thin-walled sample measuring 100 mm in height and 220 mm in length was made specifically for the tensile test. All thin-walled samples were created using the same process parameters, which included a welding current of 120 A, a voltage of 20 V, and a travel speed of 400 mm/min. Thin-walled sample construction calls for the use of shielding gas, specifically 15 L/min Argon 99.99%.

According to (Le et al., 2021) Commercial 308L steel wire with a 1 mm diameter and SS400 steel plates with dimensions of 150 mm in width, 250 mm in length, and 10 mm in thickness are used in the GMAWAM process. Table 1 lists the wire's and substrate's chemical composition. A Panasonic device (YD-350GR3) supplied the electricity for the welding heat source. The wire feed speed in this GMAWAM system automatically changes in response to the welding current, increasing as the welding current rises. A 6-axis Panasonic TA1400 robot moves the welding torch along the deposition path. A shielding gas with a 99.99% argon content was used during the welding process, flowing at a rate of 15 L/min. Following the deposition process, the sample is allowed to cool naturally in the air, returning to room temperature.

Table 2.3 Three levels of processing parameters.

Parameter	Levels		
Welding current, I (A)	100	120	140
Voltage, U (V)	17	20	23
Travel speed, v (mm/min)	300	400	500

A single weld seam wall was deposited using a 6.35 mm thick stainless steel plate (type 304) as the substrate. Standard stainless steel welding wire more precisely, Airgas USA, LLC's type ER308 LSI, 0.889mm diameter is used in this procedure. For the duration of the project, the welder operates at 22 volts and maintains a wire flow of 5,435 mm/min, or 214 IPM. A variable current was employed in conjunction with a 152 mm/min nozzle travel speed. The resulting printed wall measures 6.35 mm in thickness, 115 mm in height, and roughly 380 mm in length. There is excess material at the start of the weld pass and weld flow at the end of the deposition process because every weld pass is methodically deposited in the same direction. A tri-gas mixture consisting of 90% helium, 7.5% argon, and 2.5% CO₂ was utilised as the shielding gas during deposition, with a gas flow rate of 44 CFH. (Haden et al., 2017).

Based on the experiment, (Laghi et al., 2020), using ER308LSi wire, a thorough testing campaign was carried out to assess flat samples taken from panels made using the wire arc additive manufacturing (WAAM) process. Ten nominally $380 \times 380 \times 4 \text{ mm}^3$ panels were produced by the MX3D installation. About the deposited layer, the samples for testing are removed from these plates in three main directions: (i) longitudinally (L), aligned parallel to the deposited layer; (ii) horizontally (T), placed perpendicular to the deposited layer; and (iii) diagonally (D), placed at a 45° angle to the deposition.

2.6 Stainless steel

The article by (Jin et al., 2020), gives a thorough explanation of metal arc additive manufacturing (WAAM) for stainless steel, emphasizing how popular this process has become because of the material's advantageous mechanical characteristics and corrosion resistance. The assessment examines the defects, mechanical characteristics, and microstructure related to various grades of stainless steel as well as process variables. It talks about how the mechanical characteristics of WAAM stainless steels are affected by method, the composition of the material, parameters of the process, shielding gas, thermal following treatment, the microstructure, and defects.

To maximize the parameters and fine-tune the microstructure, more investigation into the fundamental physical processes of WAAM metallurgy and thermal post-treatment is necessary. Anisotropy is efficiently reduced by the novel WAAM + in-situ rolling process, which minimizes residual stress and distortion.

Large stainless-steel parts can now be produced at a reasonable price with WAAM. Aspects including appearance, structural growth, heat treatment effects, as well as mechanical characteristics for WAAM stainless steel components are examined in recent research. Wire speed, and examining speed, welding current, cooling time, and interlayer temperature are some of the factors that affect appearance; more research is necessary for optimization.

The structure of WAAM parts is influenced by temperature changes during manufacturing, especially the balance between austenite and ferrite phases. Control of manufacturing temperature, the use of double wires, or employing heat treatments can achieve the desired structure. Understanding how materials, manufacturing factors, and heat treatments impact the final structure of WAAM stainless steel parts is essential.

2.7 Mechanical Properties

A material's reaction to applied forces or loads is defined by its mechanical properties. They are essential for designing and engineering components in a variety of sectors because they give helpful details on how the material behaves under various circumstances. For manufactured items to be reliable, operate well, and have structural integrity, it is crucial to understand a material's mechanical properties.

2.7.1 Tensile Test

A destructive testing method called tensile testing is used to evaluate a material's mechanical characteristics, particularly how it reacts to tensile forces. This test's primary goal is to determine the material's tensile strength, yield strength, and ductility under various loading scenarios.

The material samples are subjected to progressively higher loads till the material reaches the breaking point during tensile testing. The test assesses how resistant a material is to bend and deform before cracking. Key aspects measured during tensile testing include tensile strength (maximum stress a material can withstand before breaking), yield strength (stress at which a material begins to plastically deform) and ductility (the degree to which a material can deform before failure). Determining a material's characteristics, maintaining quality, and making sure it satisfies design requirements all depend on tensile testing. Tensile testing is used by several industries, such as manufacturing and construction, to assess a material's suitability for a given purpose.

Based on the experiment that was conducted by (L. Wang et al., 2019), the specimens, which came from the middle layer of the component that was additively manufactured,

experienced both plastic and elastic deformation before breaking. Interestingly, all samples showed ultimate tensile strengths greater than 540 MPa. When compared to its SpeedPulse additively manufactured equivalent, the SpeedArc additively manufactured component showed greater tensile strength and elongation along the horizontal direction.

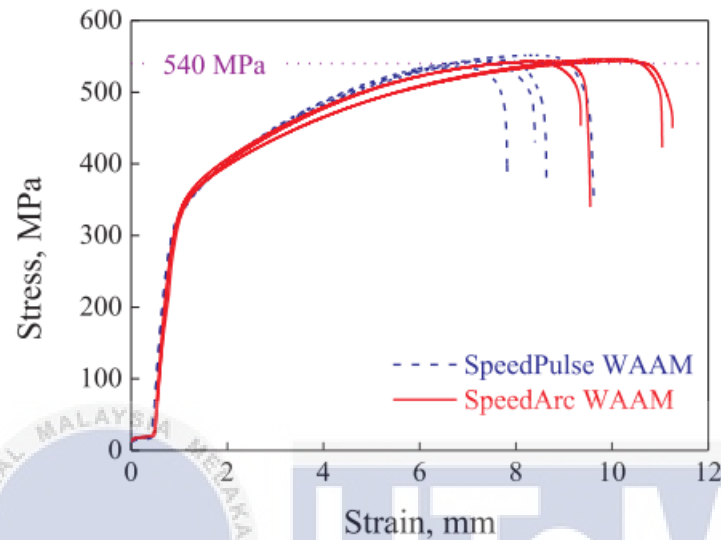


Figure 2.13 Stress-strain curves graph of SpeedPulse and SpeedArc tensile specimens along the horizontal direction. (L. Wang et al., 2019)

Specimens were taken from the bottom, middle, and top regions of the as-deposited SS316L wall for tensile tests at room temperature. Using a wire-cut Electrical Discharge Machine (WEDM), specimens were cut out following the ASTM E8 standard. Specimens from all three regions showed plastic deformation before failure. The resulting tensile characteristics were almost identical to those of their wrought alloys, as shown in Table 2.4. (Senthil et al., 2023).

Table 2.4 Tensile properties of WAAMed SS316L.

Tensile properties of WAAMed SS316L.

Tensile Property	UTS (MPa)			YS (MPa)			Elongation (%)		
Sample	Top	Middle	Bottom	Top	Middle	Bottom	Top	Middle	Bottom
Observed Value	504	507	512	197	201	205	49.5	52.1	56.5
Mean Value	507.66			201			52.7		

To assess the elasticity and ultimate tensile strength of printed stainless steel and mild steel materials—two crucial factors in design criteria—tensile testing is a must. The yield strength of stainless-steel samples was found to be higher than that of 304 wrought stainless steel (Figure 2.14), with an initial linear elastic region seen at the onset of load application (Figure 2.13, black line). An increasing trend in yield strength is observed in the X direction (direction of weld deposition) and Z direction (direction of height) when samples from various locations within the wall are analysed. The yield stress variations, which are particularly noticeable between the samples of the top and bottom walls, demonstrate how much the local thermal history and solidification regime have influenced the material properties. The wrought 304 stainless steel's UTS range is either exceeded or falls within the printed stainless steel's ultimate tensile strength (UTS, Figure 2.16) range. Notably, there is a slight increase in UTS between the upper and lower halves of the wall, and the lower half exhibits a similar response at the start and finish of the queue. Although more samples are required for statistical significance, these results imply that Wire Arc Additive Manufacturing (WAAM) UTS stainless steels can demonstrate robustness over the material's thermal history. These findings, however, demonstrate how meticulous toolpath planning can be used to regulate and engineer local material properties in the WAAM process. (Haden et al., 2017).

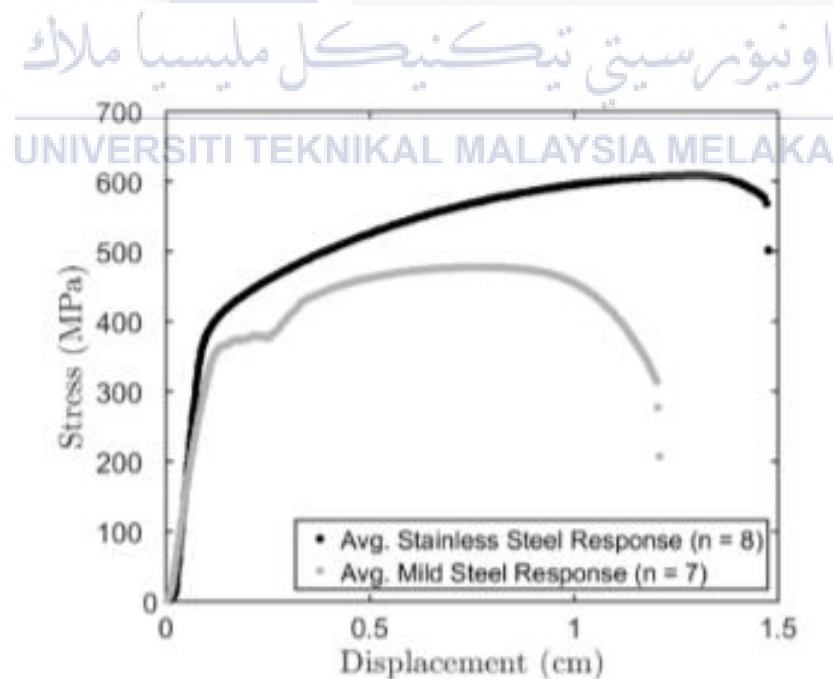


Figure 2.14 Stress-displacement curves for specimens of stainless steel and mild steel. (Haden et al., 2017)

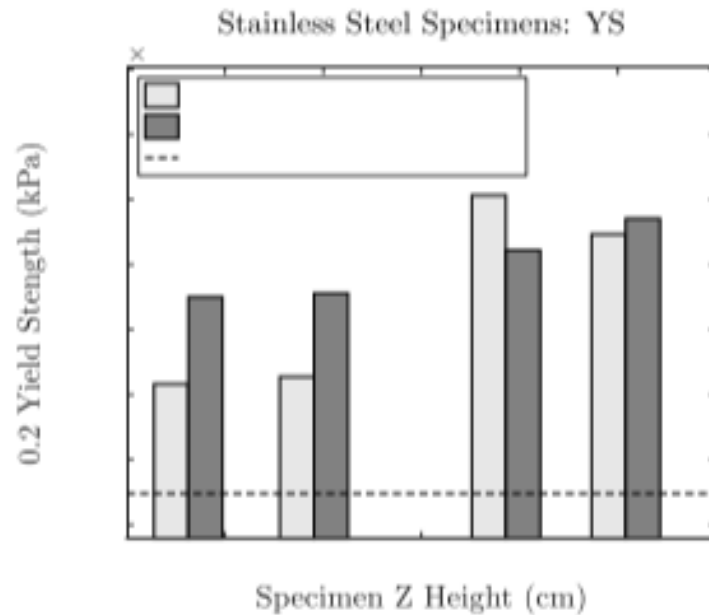


Figure 2.15 Yield strength (Haden et al., 2017)

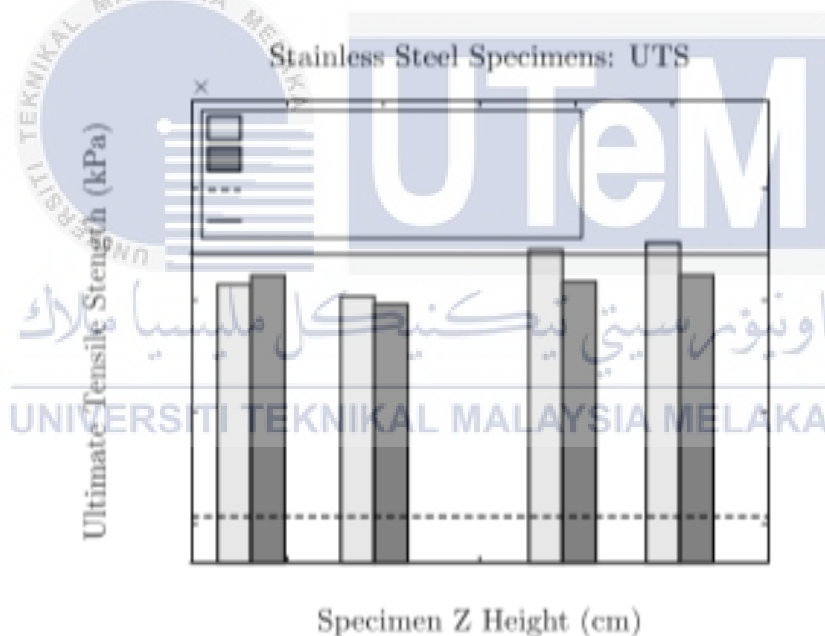


Figure 2.16 Ultimate tensile strength (Haden et al., 2017)

Based on the experiment by (Laghi et al., 2020), After surface milling samples L, T, and D to lessen the inherent roughness in the WAAM process, tensile tests were conducted. With sample D showing the highest elastic and plastic properties, the anisotropy of the tensile properties becomes clear. This phenomenon is believed to be caused by crystallization and mechanical fibrillation, which increase the density of barriers (cell

boundaries) that prevent dislocation sliding. Interestingly, dislocation sliding is more common in the D samples and preferentially occurs at a 45° angle to the tensile load.

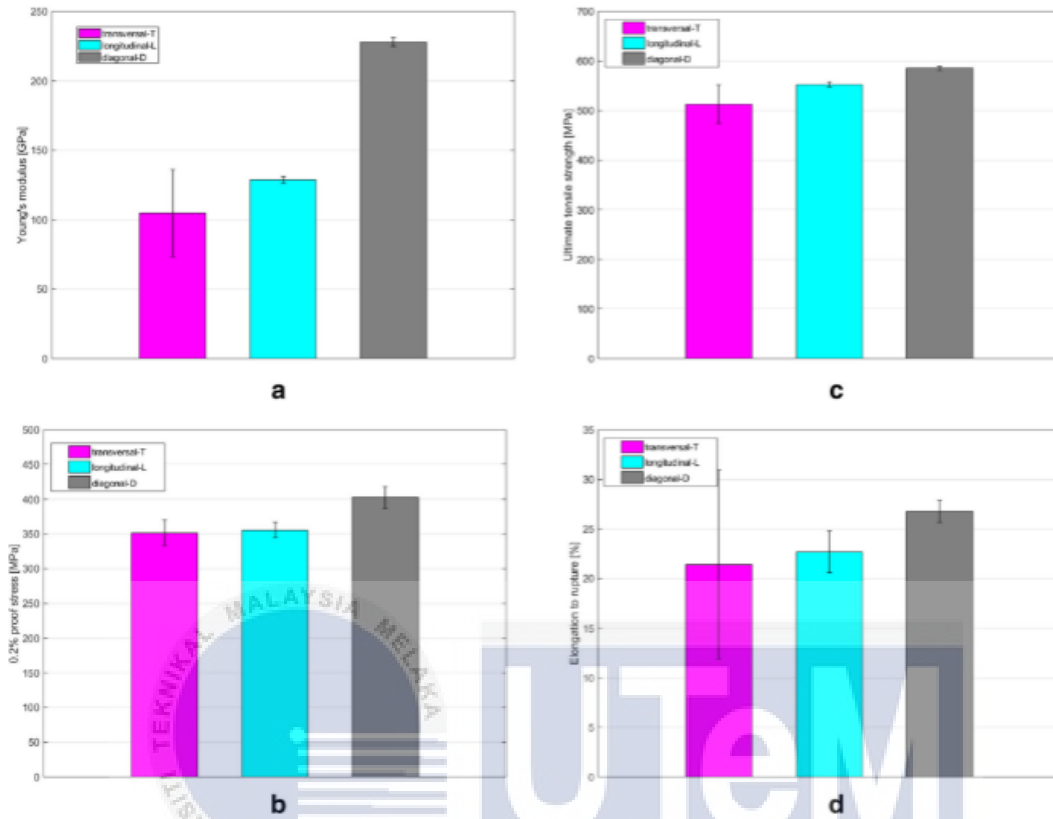


Figure 2.17 (a) Results of the tensile test specimen on L, T and D, (b) 0.2% proof stress, (c) ultimate tensile strength, (d) elongation. (Laghi et al., 2020)

2.7.2 Impact Test

One method for determining a material's resistance to shock loading or sudden force is an impact test. It gauges the material's reaction to impact, revealing details about its toughness and ability to withstand fractures. Pendulum and drop weight tests are the two primary impact test types that are frequently used. Examples of pendulum-type impact tests include the Izod and Charpy tests, in which a standard specimen is struck by a pendulum with a controlled weight. By calculating the energy absorbed by the material during impact, these tests aid in determining how impact-resistant or tough the material is. Impact testing is valuable in many industries, including construction and manufacturing, because it is essential for comprehending the way materials act according to unexpected and dynamic loading conditions.

Charpy impact test specimens measuring 55 mm x 10 mm x 3.3 mm were made in compliance with ASTM E23-02a guidelines. In the centre of the test specimen, a 45-degree angle was used to cut a V-shaped groove with a diameter of 2 mm and a root radius of 0.25 mm for the impact test. The tests are carried out at room temperature. All samples in the upper, middle, and lower regions underwent impact tests. The samples in the upper, middle, and lower regions have values of 25.8 J, 26.2 J, and 27.8 J, respectively, according to the obtained results. The standard value of 26.6 J, when tested at full size, indicates greater durability than the forged SS 316 L used in commercial settings. There was a minor variation noted in the effect on values. The lower region's value is marginally higher than the values found in the middle and upper regions. Because of the atmosphere and the cold plate, the lower region experiences extremely high rates of cooling. Consequently, there is a minor rise in values in the lower area. (Vora et al., 2022).

2.7.3 Hardness Test

By applying pressure with a harder material, a harder material is usually pressed into the material to determine its resistance to permanent deformation at the surface. This evaluation aids in analyzing the mechanical properties of metallic substances and other materials. Numerous hardness test types exist, such as the Vickers, Rockwell, Brinell, Mohs, Shore, and Knoop tests. Every test technique has its own set of guidelines and uses, making it possible to fully comprehend the hardness of a material.

Based on the experiment that was conducted by (L. Wang et al., 2019), hardness tests were carried out on the additively produced components at intervals of 2 mm, beginning with the bottom layer and ending at the top layer. The components of SpeedPulse and SpeedArc had Vickers hardness values greater than 175 HV. Interestingly, SpeedArc WAAM benefits from the effective dissipation of heat by its substrate during bottom layer deposition, exhibiting a marginally lower heat input than SpeedPulse WAAM. As a result, there is no discernible difference between SpeedArc and SpeedPulse WAAM in the bottom layer's SDAS (Secondary Dendritic Arm Distance). The Vickers hardness of the bottom layer of the SpeedPulse and SpeedArc components did not significantly differ from one another, but after the top layer was deposited, things took a different turn. SpeedArc WAAM

has a marginally lower heat input than SpeedPulse WAAM, but because of its weaker heat path and dissipation effect, it has a smaller SDAS in the bottom layer. This leads to higher Vickers hardness in the bottom layer of parts produced by SpeedArc WAAM compared to SpeedPulse WAAM, as indicated by the Hall-Petch relationship.

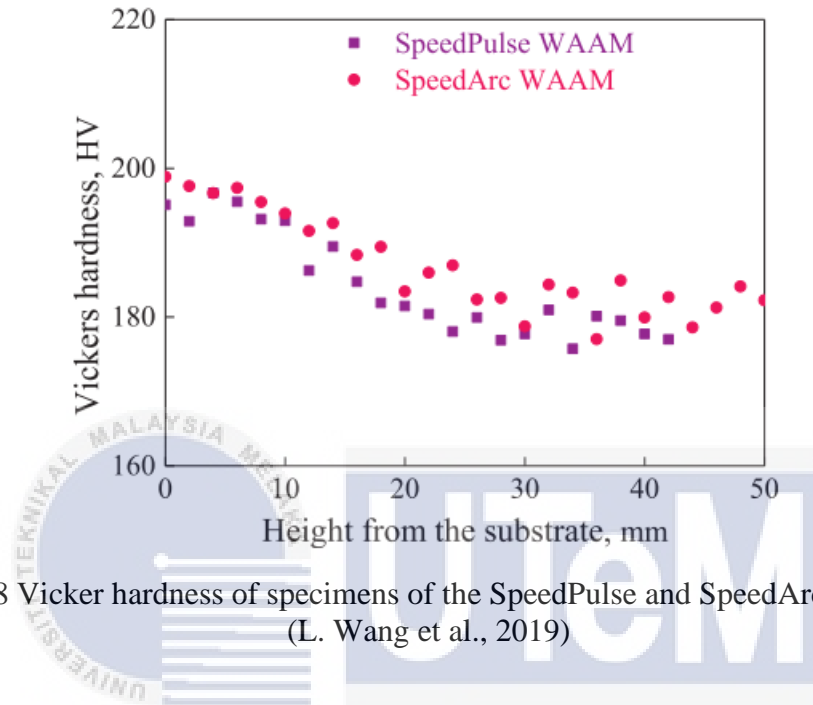


Figure 2.18 Vicker hardness of specimens of the SpeedPulse and SpeedArc components.
(L. Wang et al., 2019)

The microhardness evaluation of the SS316L wall along the direction of construction, as illustrated in Figure 2.19, reveals different values measuring 226.18 Hv, 222.03 Hv, and 217.98 Hv for the lower, middle, and upper regions, respectively. Because stiffness variations are specific to a particular location on the wall, it is easier to identify them when multiple cross-sections are used. As mentioned in the reference, heat buildup during processing still causes higher temperatures even in the presence of argon, a protective gas for cooling. Slower cooling rates are the result of heat transfer tending to concentrate through previously deposited layers as building height increases. Extended exposure to elevated temperatures will enhance the microstructure's roughness. As a result, hardness values typically increase in areas nearer the substrate and decrease in areas farther from it. (Senthil et al., 2023).

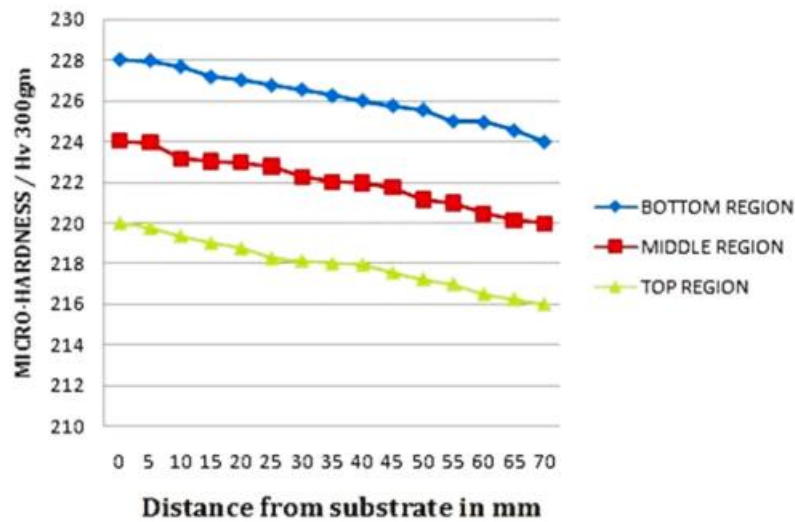


Figure 2.19 Hardness distribution along the build direction of the sample.(Senthil et al., 2023)

(Haden et al., 2017), a one-way ANOVA revealed that the microhardness values significantly increased along the same path, with a significance level of $p < 0$. The process involved a mean (μ) of 202.3 HV and a standard deviation (σ) of 5.82 HV for the initial state, and 210.9 HV and a standard deviation of 5.91 HV for the final state.

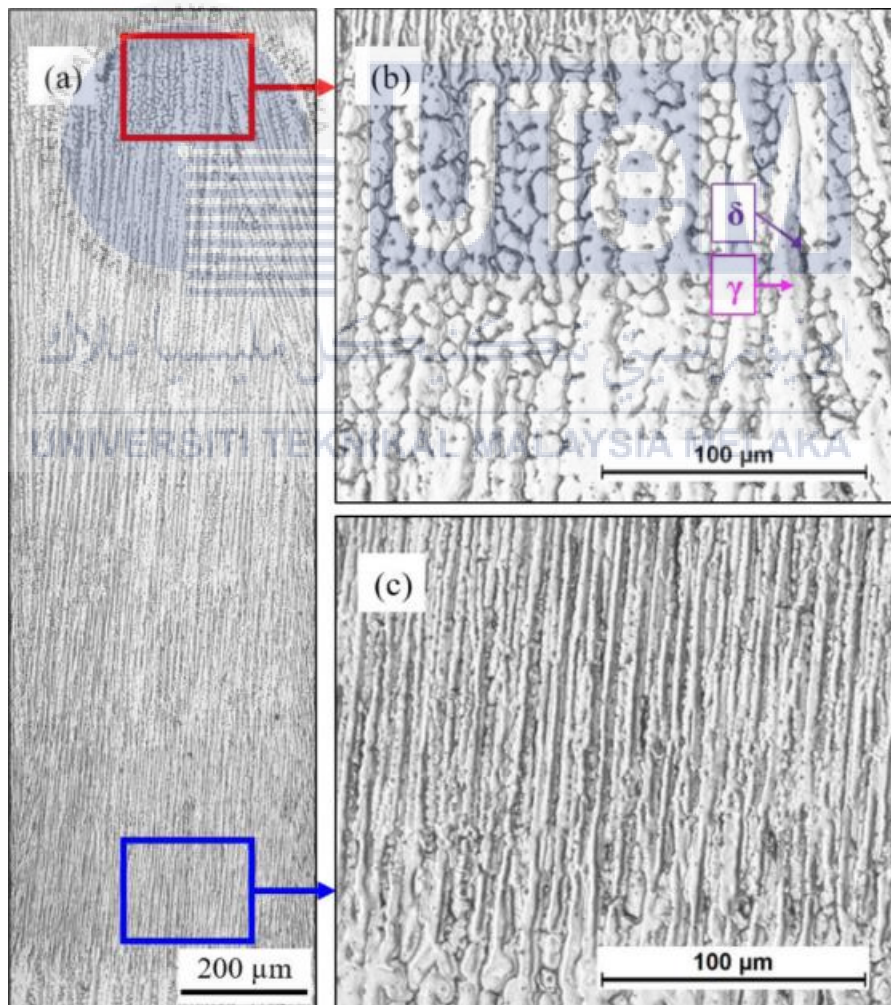
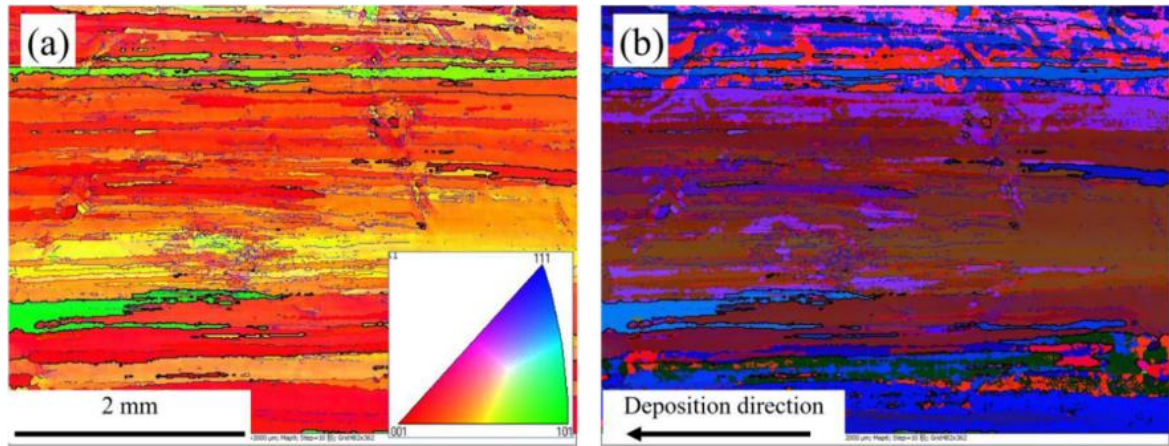
2.8 Microstructure Analysis

Microstructure analysis is the process of analysing and characterizing a material's extremely small-scale structure as shown by metallography, optical microscopy, and scanning electron microscopy, among other methods. A material's microstructure, which consists of characteristics like phases, inclusions, defects, and grain boundaries, can reveal important information about its characteristics and behaviour. Knowing how one organizes these microscopic components affects a material's performance and properties is crucial to the field of materials science.

Based on the experiment that was conducted by (L. Wang et al., 2019), Figures 2.20, 2.21, and 2.22 provide a detailed analysis of the microstructure of components produced by SpeedArc WAAM. In Figure 2.20, an Electron Backscattered Diffraction (EBSD) map reveals grain orientation, with most grains aligning along the 001 direction, indicating a vertical growth orientation. The austenite (γ) distribution map in Figure. 2.20(b) confirms that the primary phase of the WAAM component is austenite.

Moving to Figure 2.21, optical micrographs depict a specific layer of the wire arc additive manufactured component. Ferrite (δ), shown in grey, distributes within the austenite (γ) matrix in white. Higher magnification micrographs in Figure 2.21(b) and (c) illustrate grain growth along the vertical direction, with observed cellular structures near the fusion line developing into fine columnar and then coarse columnar structures.

Figure 2.20 compares microstructures from central transverse sections of components produced by SpeedPulse and SpeedArc additive manufacturing at different layers. This allows meaningful comparison, emphasizing the impact of the metal transfer mode on microstructure. The evaluation metric, Secondary Dendrite Arm Spacing (SDAS), plays a crucial role, as smaller SDAS correlates with improved mechanical properties in arc additive manufacturing components.



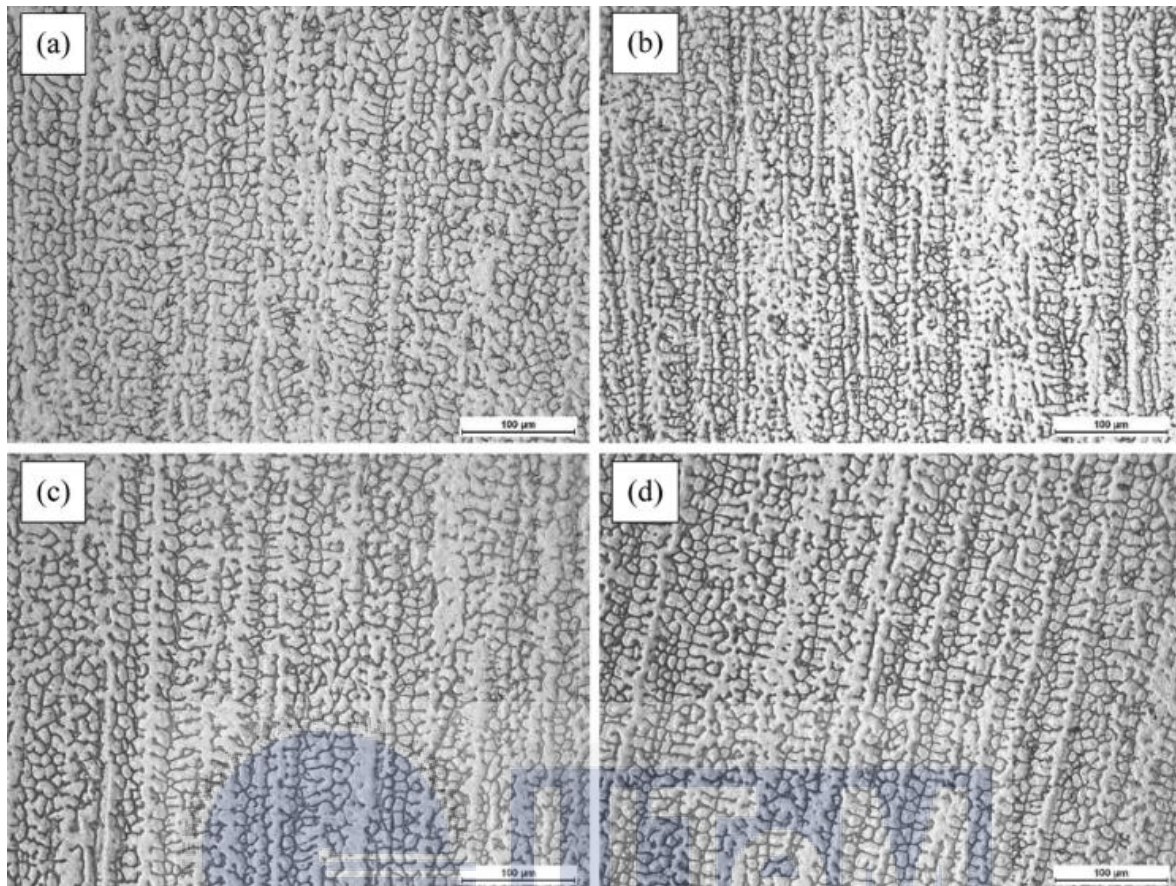


Figure 2.22 Optical metallurgy graphs at the transverse cross-section of the components.
(L. Wang et al., 2019)

According to (Senthil et al., 2023), the optical micrograph during the additive manufacturing process reveals unique features within the manufactured wall. Fine equiaxed dendrites are seen in the bottom region, and columnar grains with leftover δ -ferrite are seen in the middle region. There is a columnar dendritic structure visible in the upper region. A layer of incredibly fine columnar dendrites sits atop a layer of extremely finely equiaxed grains to form the fabricated wall itself.

To build an extra layer, the surface of the old layer must melt, combine with the molten wire feed, and then solidify. Because of the significant temperature gradient at the interface between the molten layer and the deposited layer, this new layer has fine equiaxed grains. The greatest temperature differential affects the direction in which grains grow, causing columnar dendrites to form.

This intricate process highlights how the temperature gradient plays a crucial role in shaping the microstructure during additive manufacturing, giving rise to the observed equiaxed and columnar features. Figure 2.23 shows the microstructure of the wall.

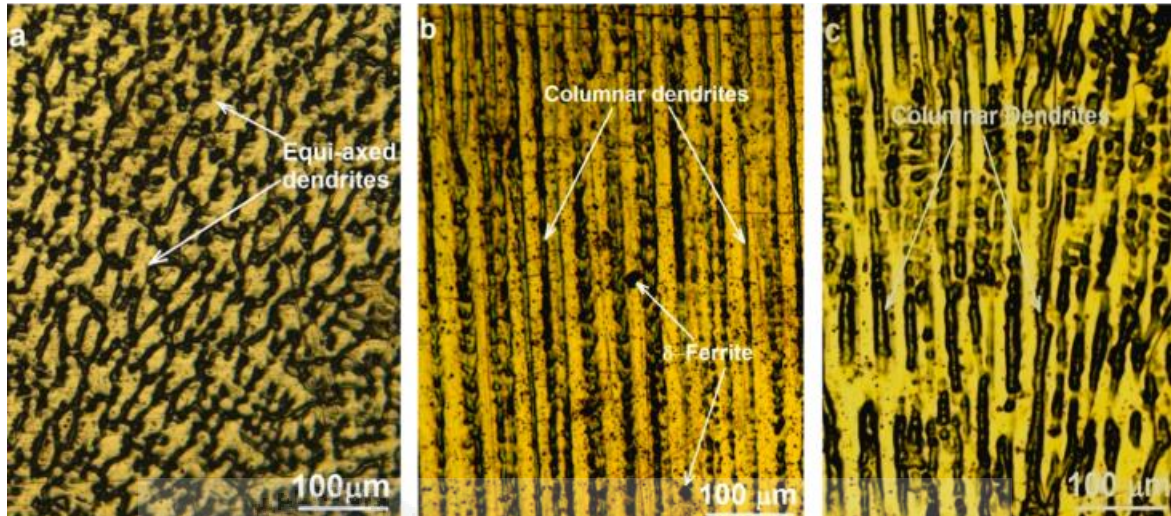


Figure 2.23 Microstructure of the wall, (a) bottom region, (b) middle region and (c) top region. (Senthil et al., 2023)

(Haden et al., 2017), The ME stainless steel samples were subjected to an optical micrograph, which demonstrated a definite microstructure boundary at the weld line interface, as illustrated on the left in Figure 2.24. Remarkably, because of obvious mixed modes of solidification, the same ME sample displays a variety of microstructures, from austenitic to solidification structures with a mixed ferrite morphology. The sudden changes in microstructure texture indicate that anisotropy is significantly influenced by local thermal histories.

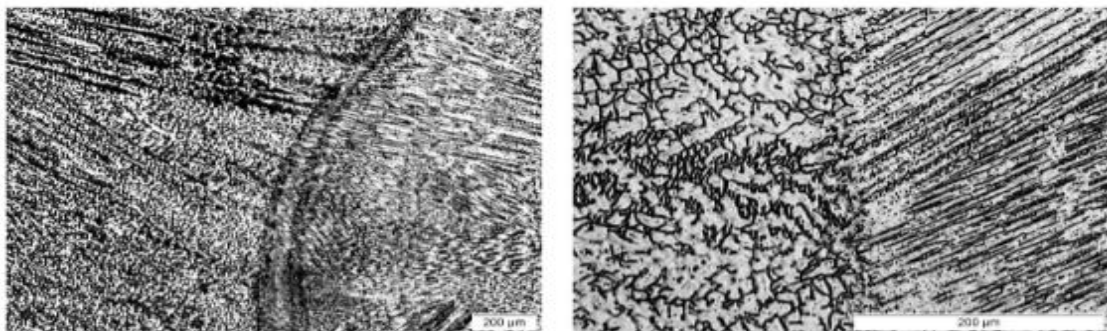


Figure 2.24 Optical micrographs of the interfacial layer between weld lines (left) and repeating microstructural shifts observed near. (Senthil et al., 2023)

(Laghi et al., 2020), the microstructural analysis revealed a distinctive hierarchical structure inherent to additively manufactured components. This structure is organized into deposition layers, featuring epitaxial columnar grains traversing across layers, accompanied by a refined cellular sub-structure within the grains.



Figure 2.25 Optical micrographs of the interfacial layer between weld lines. (Laghi et al., 2020)



2.9 Isotropy and Anisotropy

Anisotropy, within the realms of physics, material science, and geology, is a term denoting a property reliant on direction or manifesting distinctive features along multiple axes. In simpler terms, anisotropy signifies the lack of symmetry or uniformity in a substance or phenomenon concerning various directions. In the field of materials science, a material can exhibit anisotropic characteristics, indicating that its mechanical, electrical, or thermal properties vary based on the direction of measurement.

In contrast, isotropy characterizes a condition where a phenomenon, system, or property demonstrates uniformity, presenting identical features in all directions. Simply put, an isotropic substance or system showcases symmetry along all orientations or axes. Within the realm of material science, isotropic materials possess consistent mechanical, electrical, and thermal traits in every direction. Consequently, an isotropic material would exhibit uniform behavior and maintain consistent strength, regardless of the magnitude of applied force.

Anisotropy, in contrast to isotropy, refers to the lack of symmetry or uniformity across different orientations within a substance, phenomenon, or system. Therefore, anisotropy signifies characteristics that vary or depend on direction, while isotropy indicates a state of complete uniformity.

Previous studies such as (Hadjipantelis et al., 2022) showed anisotropy in the mechanical response of WAAM stainless steel, indicating that certain factors influence its behaviour. Similarly, (C. Wang et al., 2022), conducted a comparative study on 316 stainless parts produced by WAAM, highlighting the anisotropy of microstructure and mechanical properties.

CHAPTER 3

METHODOLOGY

3.1 Introduction

To investigate the mechanical characteristics and microstructural characteristics of austenitic stainless steel 308LSI produced through wire arc additive manufacturing (WAAM), this study uses an experimental methodology. The research design makes use of several experiments to evaluate utilizing microstructural analysis and mechanical properties. Sample preparation and WAAM structure fabrications are all included in the methodology.



3.2 Flow Chart

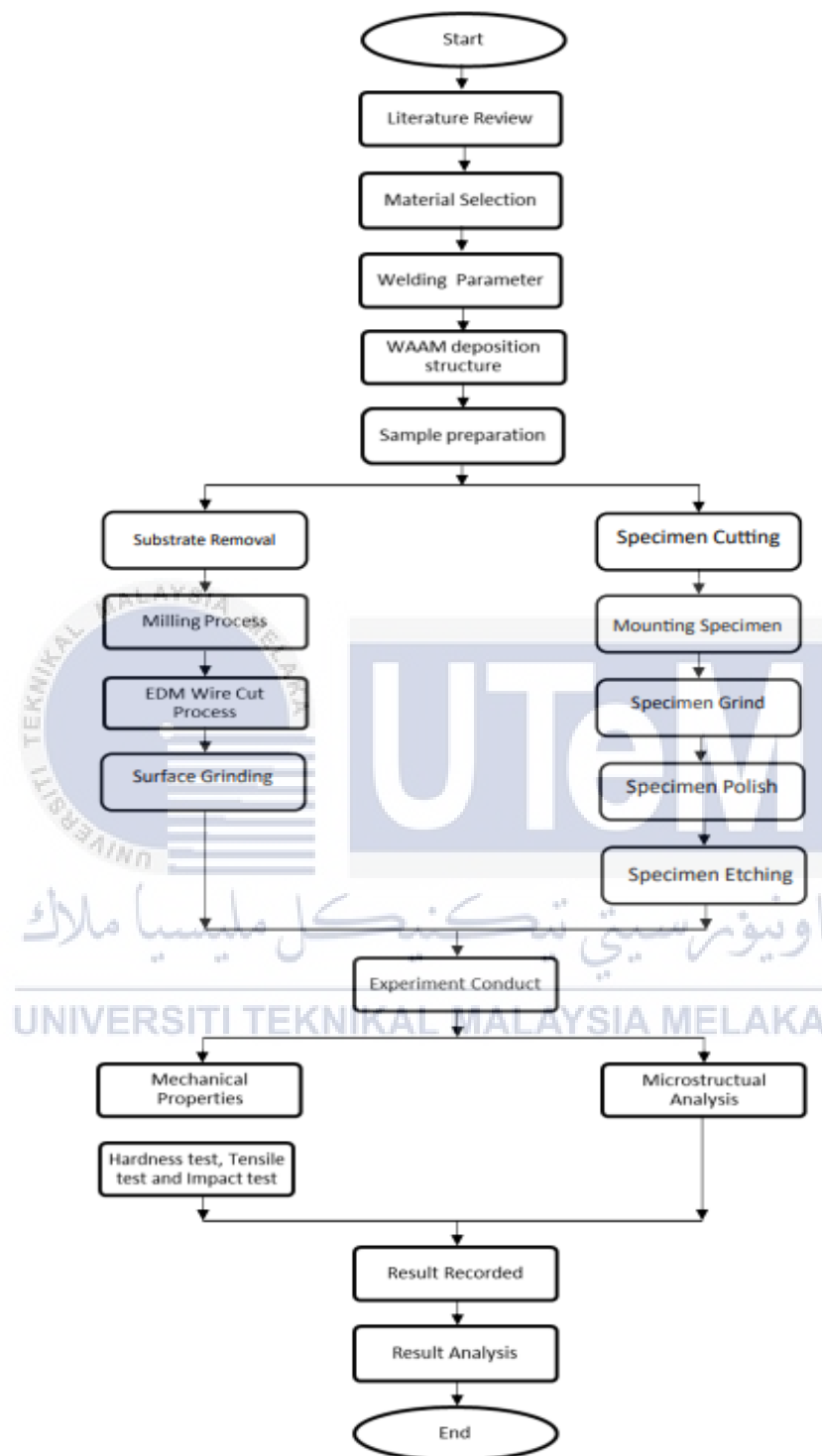


Figure 3.1 Flow chart

3.3 Materials

Metals such as steel, stainless steel, aluminium, titanium, and copper alloys are among the materials that WAAM can use. The material selection is based on the particular application needs and the desired finished component properties.

3.3.1 Stainless Steel 304 (Substrate)

The most popular and adaptable stainless steel alloy is stainless steel 304. Because it is an austenitic stainless steel, it contains a lot of nickel and chromium. Because of this, 304 stainless steel has exceptional strength, formability, and resistance to corrosion. It is a well-liked option for a variety of applications because it is also reasonably priced. Other benefits of stainless steel 304 include its good heat conductivity, which contributes to even heating of the substrate and the material that is deposited. Moreover, stainless steel 304 has a low value of thermal expansion, which lessens residual stress in the deposited material and is a good electrical conductor, both of which are critical for forming a stable arc during the WAAM process. The size of the substrate that we used was 100mm x 50mm x 8 mm.



Figure 3.2 Stainless steel 304 (substrate)

3.3.2 Stainless Steel 308LSi (Filler wire)

SS308LSI is a type of austenitic stainless steel welding wire that is used in a variety of welding applications. It is a stainless steel from the 308 series, which is often used for welding similar or dissimilar stainless steels, as well as attaching stainless steel to carbon steel.

The low carbon content of SS308LSI helps to reduce the risk of intergranular corrosion and sensitization during welding. It is also stabilised with titanium (Ti) and niobium (Nb), which enhances its resistance to intergranular corrosion even further.

The "LSI" in SS308LSI stands for "Low Silicon Iron," meaning that the wire has a small amount of silicon. During welding, silicon is known to encourage the development of silicon-rich oxides, which can result in weld defects and reduce mechanical characteristics. The low silicon concentration of SS308LSI reduces the possibility of such problems and assures high-quality welding.

SS308LSI wire is most used in GMAW or MIG welding techniques. It can be used for welding in a variety of industries, including automotive, construction, food processing, and chemical processing. Joining stainless steel tanks, pipes, structures, and equipment is common.

When used properly, SS308LSI wire produces welds with high corrosion resistance and mechanical properties that closely match the base metal. It is weldable and can be utilised in single-pass and multi-pass welding techniques. To achieve high-quality welds with SS308LSI wire, proper welding techniques, such as appropriate heat input, shielding gas selection, and weld preparation, are required, as with any welding process.

Finally, SS308LSI is an austenitic stainless steel welding wire grade that is commonly used in welding applications to join stainless steel and stainless steel to carbon steel. Its low carbon and silicon percentage helps to improve corrosion resistance and reduce weld flaws. SS308LSI wire is essential in the fabrication of robust and corrosion-resistant welded structures and equipment because of its outstanding weldability and compatibility with various welding techniques. The brand of this wire is DRATEC Drahttechnik GmbH and the diameter of the wire is 1.20 mm.



Figure 3.3 SS308LSi (filler wire)

Table 3.1 Chemical Composition of SS308LSi filler wire.

Element	C	Si	Mn	Cr	Ni
%	0.02	0.85	1.75	19.0	9.5

Table 3.2 Mechanical Properties of SS308LSi filler wire

Yield Strength	390 N/mm ²
Tensile Strength	590 N/mm ²
Elongation	35%
Impact Energy	80J
Highest Operating Temperature	350 °C
Lowest Operating Temperature	-196 °C

3.4 Parameters

Important welding process variables must be selected and closely watched during the WAAM process. The wire feed rate, voltage, and current are these parameters. Together, these variables will have an impact on the heat input during the welding process, which will have an impact on the welding properties.

Table 3.3 Parameter of welding.

Sample	Current (Amps)	Voltage (V)	Wire Feed Speed (m/min)	Heat Input (J/mm)
1	65	9.9	1.8	21.45
2	75	10.3	2.3	21.15
3	85	10.5	2.6	20.60
4	95	10.8	3.0	20.52
5	105	11.6	3.5	20.88
6	115	11.6	4.0	20.01

$$\text{Heat Input} = (\text{Voltage} \times \text{Current} \times 60) / (\text{Wire Feed Speed} \times 1000) \quad (2.1)$$

The parameters that we choose are 115A, 11.6V and 4.0 m/min.

Table 3.4 Parameter for welding

Current (A)	115
Voltage (V)	11.6
Wire feed speed (m/min)	4.0
Stick out (mm)	10.0
Shield gas composition	98 % Ar, 2 % O ₂
Shield gas flow rate (L/min)	20
Layer height (mm)	2

3.5 Experimental Setup

The ABB robot welding is used to produce the sample in this study. The steps are as follows:

- Setup: The shielding gas valve was switched on. The Cold Metal Transfer (CMT) power supply was switched on. The robot controller was switched on.



Figure 3.4 The shielding gas valve was switched on.



Figure 3.5 The Cold Metal Transfer (CMT) power supply was switched on.



Figure 3.6 The robot controller was switched on.

- b) Welding station: Mount the SS304 (substrate) the size 100mm x 50mm x 8mm on the welding station where the deposition process takes place.



Figure 3.7 Clamp on the substrate to the table.

- c) Select the parameter: The voltage was set to 15.2V, the current was set to 112A, and the wire feed speed was set to 4.2 m/min on the CMT power source.

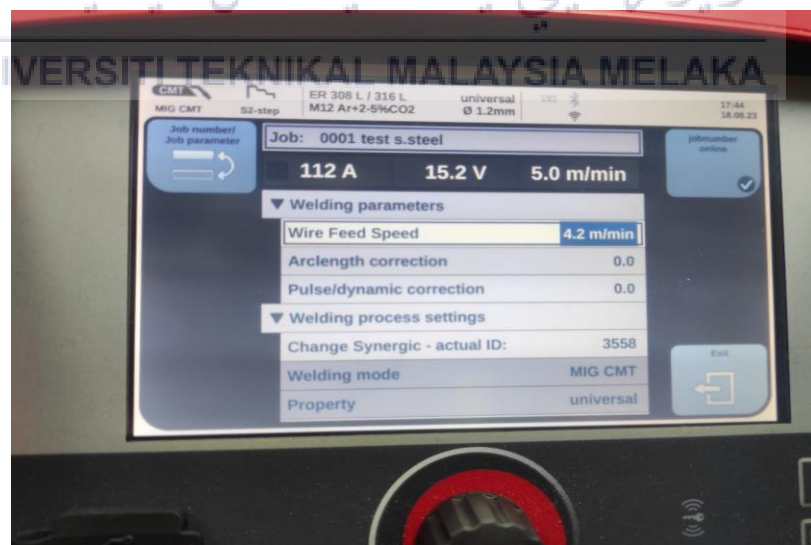


Figure 3.8 Parameter set on the CMT power source.

- d) Simulation preparation: The welding parameter was set. The current and voltage were disabled (simulation does not require the deposition process). The welding path

for the simulation was programmed from the beginning welding position to the end position. The simulation was started. The program was run

- e) Deposition Process: Use the teach pendant to enable the current and voltage. Run the program.



Figure 3.9 Deposition process.

- f) End Process: Turn off all switches and gas valves. Safely remove the structure from the table.

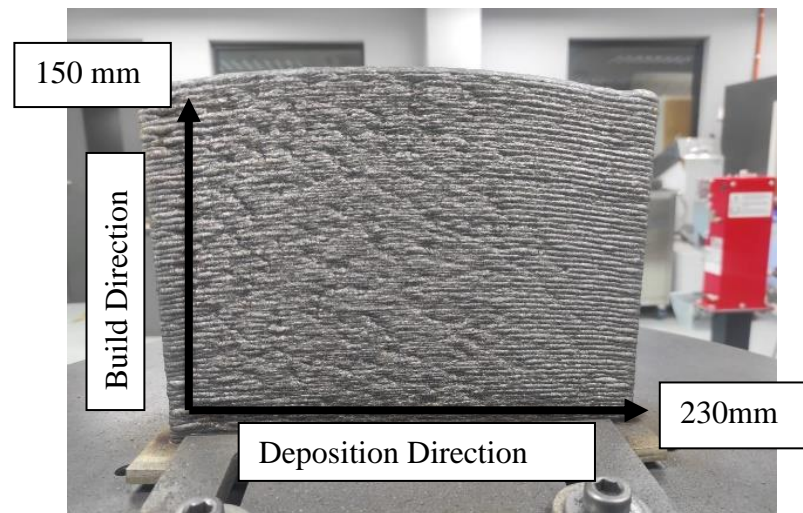


Figure 3.10 Structure fabricated from CMT WAAM

3.6 Equipment

To perform Wire Arc Additive Manufacturing (WAAM), a robot controller, robot arm, welding torch, CMT power source, and shielding gas system are required. Together, these elements make the WAAM process possible.

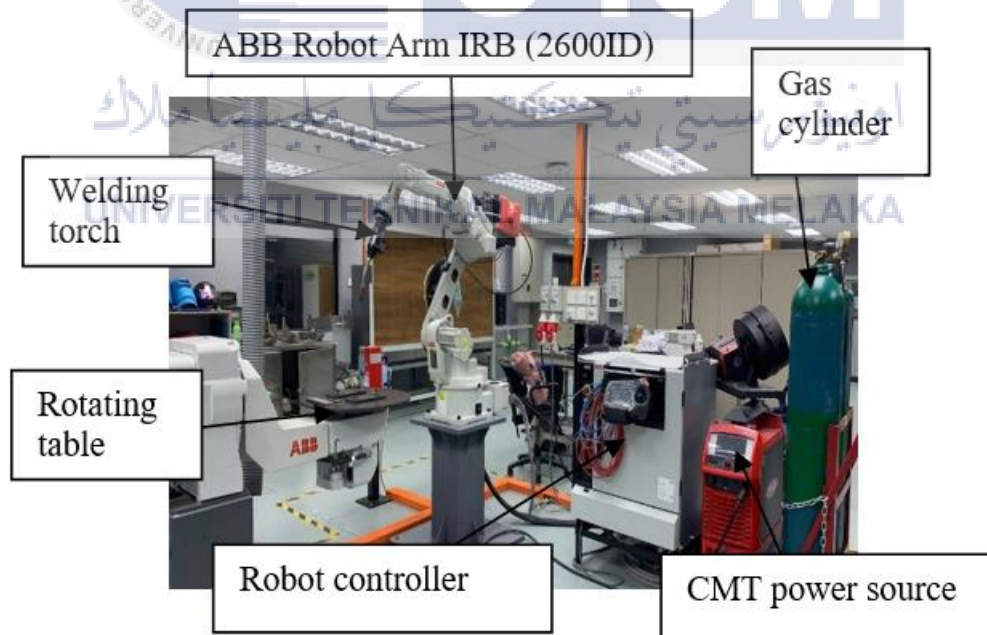


Figure 3.11 Setup of equipment that is used in the WAAM process.

3.6.1 ABB Robot Arm IRB (2600ID) and Welding Torch

Often just called a "robot," a robot arm is a mechanical device that replicates the motions of a human arm. It usually has several linked segments (joints and links, for example) that enable it to move in different directions. Robotic arms find extensive usage in various fields, such as manufacturing, where they can execute tasks quickly, accurately, and consistently. The robot arm is in charge of holding and guiding the welding torch during the welding process in robotic welding. A computing device or controller precisely controls the arm's movements to follow preset paths and produce precise welds.

The welding process is carried out by the welding torch, a mounted or portable instrument. Typically, it consists of parts like an electrode, shielding gas supply, and nozzle. The workpiece and the welding material, which is usually a metal wire or electrode, are fused by the intense heat produced by the torch. Robotic welding involves attaching the welding torch to the robot arm and controlling its movement along the welding path. To guarantee correct fusion and high-quality welding, the torch's angle, distance from the workpiece, and other settings are carefully controlled.

The welding torch and robot arm work together to create a strong, fully automated system for welding jobs. Robotic welding systems are used to increase welding precision, efficiency, and consistency while reducing human intervention in a variety of industries, including aerospace, construction, automotive manufacturing, and shipbuilding.



Figure 3.12 Robot arm and welding torch. IRB 2600ID

3.6.2 Cold Metal Transfer Power Source

Cold Metal Transfer (CMT) power source is a preferred choice for the Wire Arc Additive Manufacturing (WAAM) process due to its ability to provide controlled heat input, precise wire feeding, and dynamic welding parameter adjustments. By utilizing the CMT power source, researchers and engineers can achieve improved weld quality, reduced distortion, and enhanced process stability, making it an excellent choice for WAAM applications.



Figure 3.13 CMT power source. Fronius TPS 400i.

3.6.3 Robot Controller

The robot controller for WAAM provides precise and synchronized control of the robot's movements and welding processes. It allows for seamless integration and coordination between the robot, welding torch, and other peripherals, ensuring accurate deposition of the metal and consistent welding quality.

WAAM-specific robot controllers often come equipped with advanced motion control algorithms and path planning capabilities. These features optimize the robot's movements, enabling smooth and precise motion trajectories while maintaining the desired deposition parameters. This level of control ensures the deposition accuracy required for complex geometries and high-quality additive manufacturing.

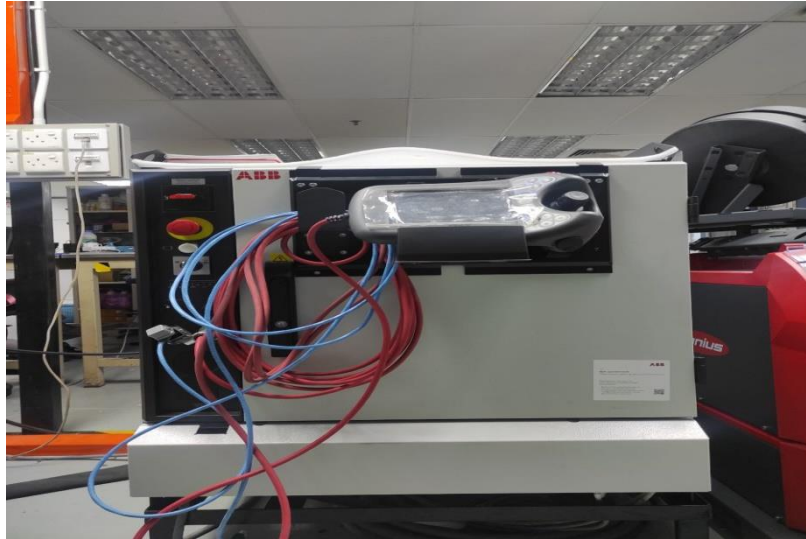


Figure 3.14 Robot Controller. IRC5 Controller.

3.6.4 Shielding Gas (Argon + O₂)

Shielding gas is an essential component in the Wire Arc Additive Manufacturing (WAAM) process, as it plays a crucial role in ensuring the quality and integrity of the fabricated components. In the case of WAAM, a common choice for shielding gas is a mixture of Argon and Oxygen (O₂).

The combination of Argon and Oxygen provides several benefits for the WAAM process. Argon, being an inert gas, helps to create a stable arc during welding. It shields the weld pool from atmospheric gases, preventing contamination and promoting a clean and sound weld. Oxygen facilitates the combustion of the wire electrode, resulting in increased heat input and a more concentrated and stable arc. This improved arc stability enables better control over the deposition process, leading to improved bead shape, reduced spatter, and enhanced overall weld quality.



Figure 3.15 Shielding Gas (Argon + O₂)

3.7 Sample Preparation

Sample preparation is an essential step in any study or analysis of materials. It involves collecting representative samples and shaping them to the desired size and shape. The samples are then prepared by milling, wire cutting and surface grinding to create a suitable surface for analysis.



Figure 3.16 Sample of WAAM.

3.7.1 Cutting Process

Cutting is a process of severing a material into two or more parts. It is a subtractive manufacturing process, meaning that material is removed from the workpiece to create the desired shape and features. Cutting can be performed using a variety of tools and methods, depending on the type of material being cut and the desired results. In this study, we use a horizontal bandsawing machine to remove the substrate from the sample.



Figure 3.17 Horizontal Bandsawing Machine PR-10V.



Figure 3.18 Cutting process (remove the substrate from the sample).



Figure 3.19 Sample after removing the substrate.

3.7.2 Milling Process

In the milling process, material is removed from a part using rotating cutters. A milling cutter is a type of rotary cutter that frequently has several cutting points. In contrast to drilling, which involves moving the tool along its axis of rotation, a milling cutter is usually moved at an angle perpendicular to its axis, allowing the cut to be made around the cutter. The cutting edges (flutes or teeth) of the tool continuously cut in and out of the material as the cutter enters the workpiece, removing chips (shavings) with each cut.

A workpiece can be made with a multitude of shapes and features using the flexible process of milling. Face milling, end milling, peripheral milling, slotting, and gear cutting are a few frequent milling operations. The speed of the face mill was 600 RPM. The excess material was removed, geometries were refined, and the desired surface finish was achieved.



Figure 3.20 Vertical Turret Milling Machine. Model FM-15S



Figure 3.21 Milling process.



Figure 3.22 Sample before the milling process.

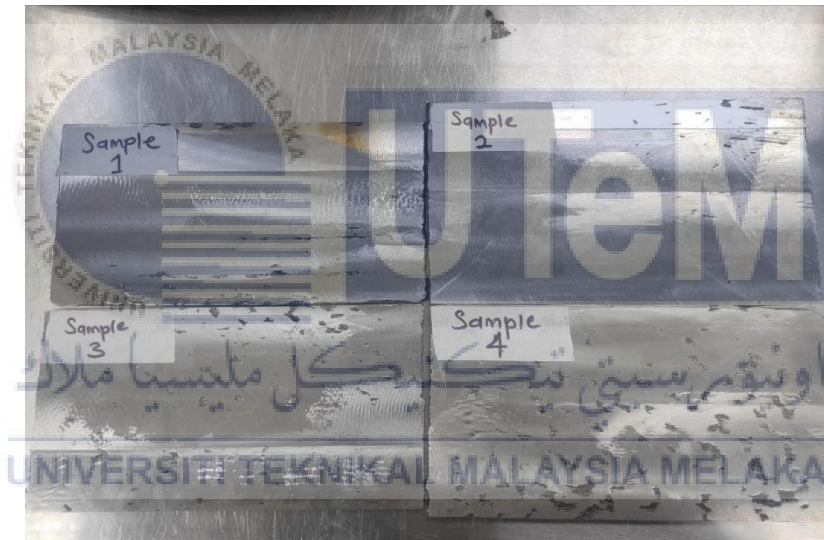


Figure 3.23 Figure 3.21 Sample after the milling process.

3.7.3 Electrical Discharge Machining (EDM)

A thin wire electrode is employed in the non-contact electrical discharge machining (EDM) wire-cutting process to cut conductive materials. A dielectric fluid, like deionized water, is submerged in the wire electrode as it passes through the workpiece. A small amount of material from the workpiece is melted and vaporised when a voltage is applied between the wire and the workpiece. As the wire electrode passes through the workpiece, this process is repeated, creating a precise, intricate shape. Hardened steel, super alloys, ceramics, and other materials can all be cut using the flexible and effective wire EDM machining technique. Moreover, it can cut intricate features and forms that are challenging or

impossible to cut using conventional machining techniques. We use EDM wire cut to cut the specimen for tensile test, impact test, hardness test and microstructural analysis.



Figure 3.24 EDM Wire Cut Sodick VZ300



Figure 3.25 0.25mm diameter Brass EDM wire

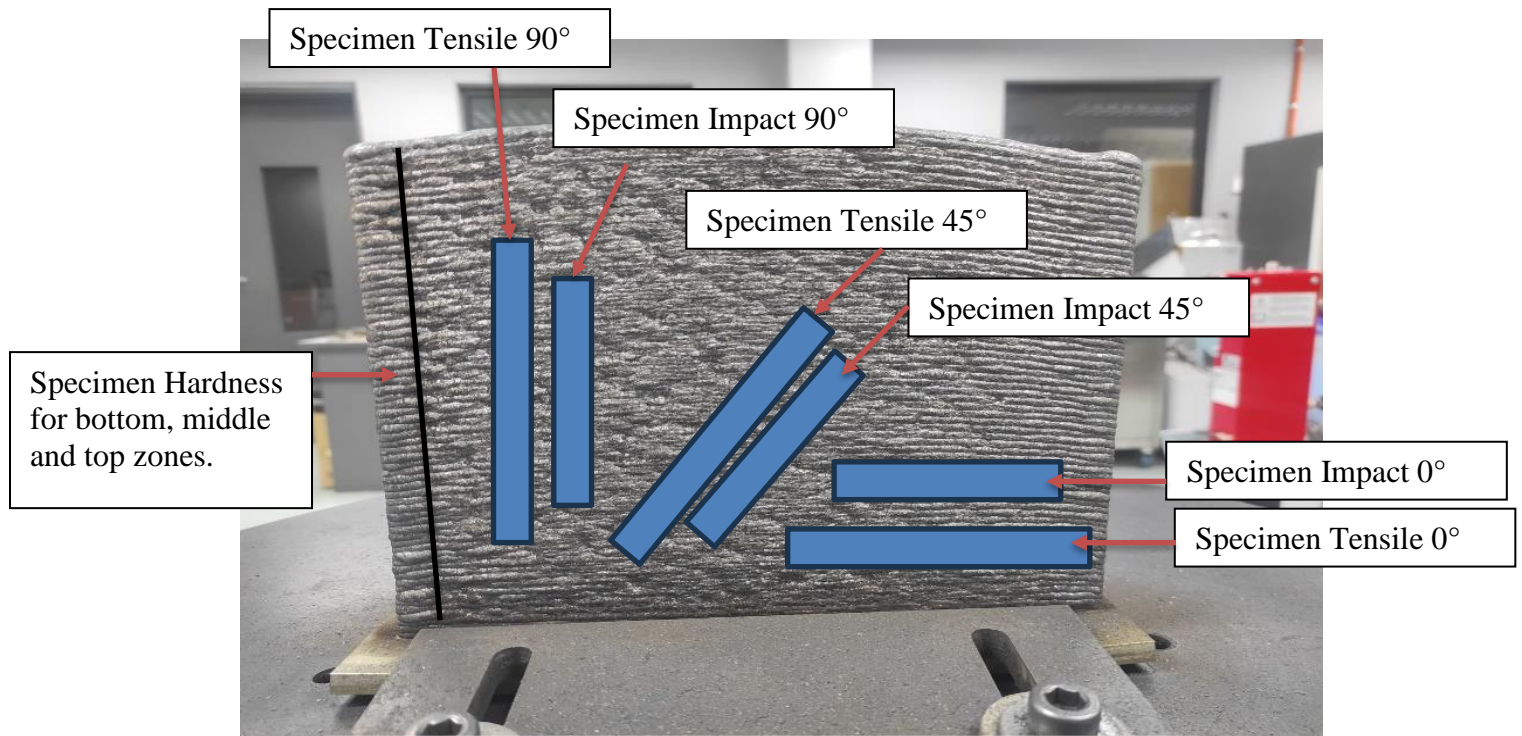


Figure 3.26 Specimen arrangement in sample

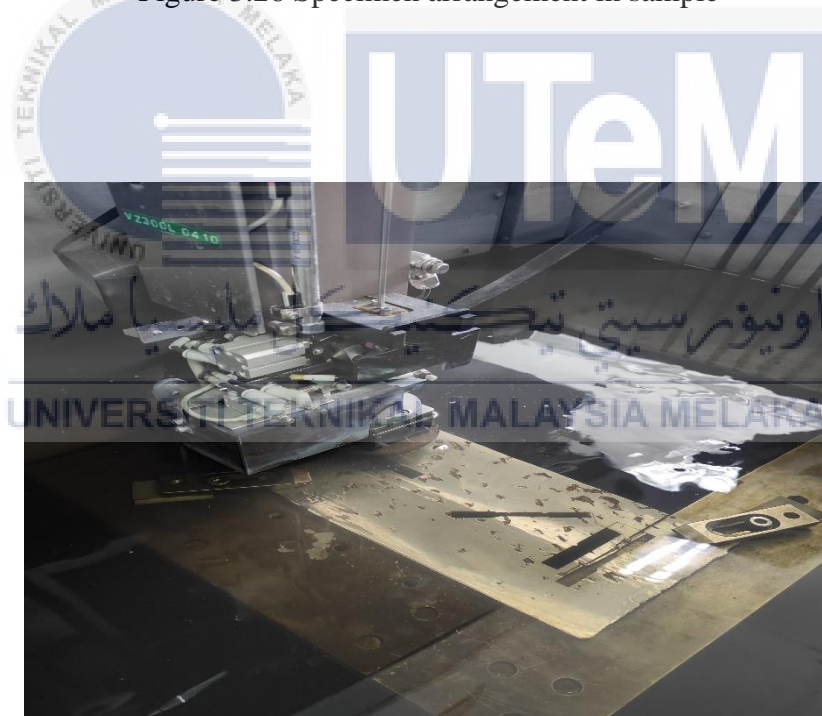


Figure 3.27 Cutting Process



Figure 3.28 Samples after the cutting process.



Figure 3.29 Impact specimen at (0°)



Figure 3.30 Tensile Specimen at (0°)





Figure 3.33 Impact specimen at (90°)



Figure 3.34 Tensile specimen at (90°)

3.7.4 Surface Grinding

A precise machining technique called surface grinding is used to give a part a smooth surface. To achieve high precision, surface finish, and dimensional control, this method is frequently employed in the production and metallurgical industries. To create a flat, smooth surface on the sample, we use grinding techniques to remove material.



Figure 3.35 Surface Grinder Proth PSGS-4080AHR



Figure 3.36 Specimen during the surface grinding process



Figure 3.37 Specimen before surface grinding



Figure 3.38 Specimen after surface grinding



Figure 3.39 Specimen of Impact Test before surface grinding process.



Figure 3.40 Specimen of Impact Test after surface grinding process

3.8 Mechanical Properties

A material's reaction to applied forces or loads is defined by its mechanical properties. They are essential for designing and engineering components in a variety of sectors because they give helpful details on how the material behaves under various circumstances. For manufactured items to be reliable, operate well, and have structural integrity, it is crucial to understand a material's mechanical properties.

3.8.1 Tensile Test

The purpose of using a tensile test machine in Wire Arc Additive Manufacturing (WAAM) is to assess and evaluate the mechanical properties of the WAAM-built structures or components, specifically their tensile strength, yield strength, and elongation.

Tensile testing is a standardised method that applies axial tension to a specimen until it fractures, allowing for the measurement of load and deformation. In WAAM, the use of a tensile test machine serves several important purposes. The tensile test helps in material

characterization by providing valuable information about the material's behaviour under tensile forces, including its strength and ductility. By conducting tensile tests on WAAM specimens, we can determine properties such as ultimate tensile strength, yield strength, and elongation, which are essential for understanding the material's performance.

The tensile testing was conducted on the specimens adhered to the ASTM E8 standard, a widely accepted guideline for evaluating the tensile properties of metallic materials. In this study, a scale-down factor of 0.75:1 was applied to the specimens, indicating a reduction of 25% in dimensions compared to the standard specifications outlined in ASTM E8. It is because the printed wall is thin. So the surface of the wall cannot be milled cleanly. That is why the reason we scale down the dimension so that it does not affect the tensile coupon. The parameter of the machine is the load capacity was 200 kN, the speed is 5 mm/min.

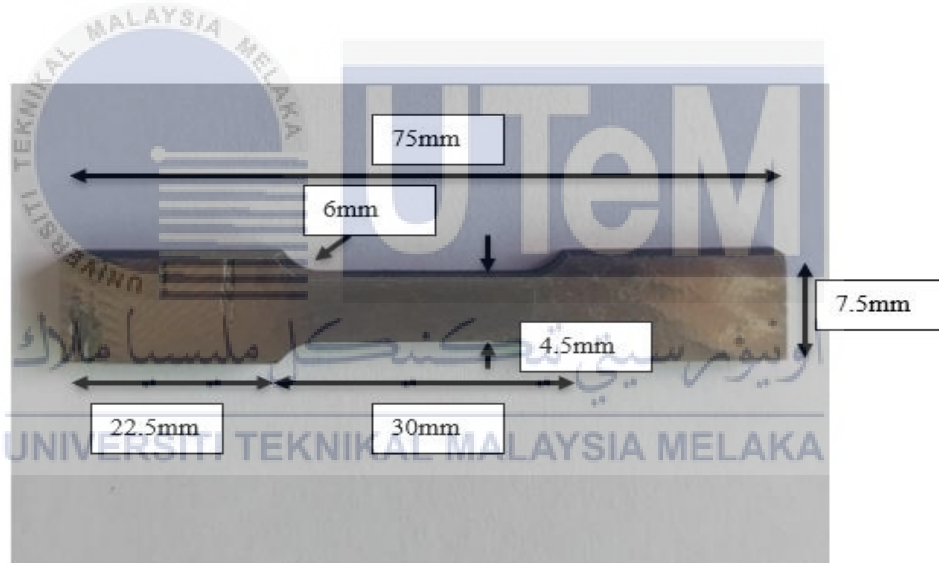


Figure 3.41 Dimension of the tensile specimen



Figure 3.42 Floor-Mounted Material Testing System. Instron Model 5585 Capacity 200KN.



Figure 3.43 Specimen of 0° before tensile test



Figure 3.44 Specimen of 0° after tensile test

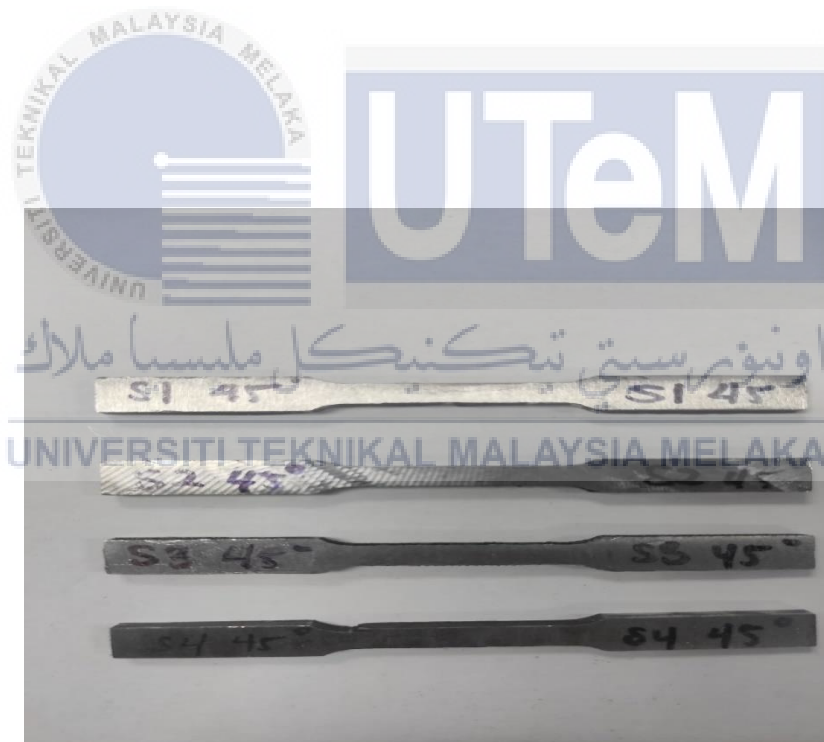


Figure 3.45 Specimen of 45° before tensile test



Figure 3.46 Specimen of 45° after tensile test



Figure 3.47 Specimen of 90° before tensile test



Figure 3.48 Specimen of 90° before tensile test

3.8.2 Impact Test

Charpy impact testing is used in Wire Arc Additive Manufacturing (WAAM) to assess the durability and impact resistance of the structures or parts produced by WAAM. A standardised technique called Charpy impact testing is used to quantify the energy that materials absorb when they are struck by a swinging pendulum, causing damage. It is crucial to assess mechanical qualities, such as impact resistance, in WAAM since the method of additive manufacturing includes the deposition for each layer of material.

Charpy testing is performed using a Universal Pendulum Charpy Impact Tester, 500 Joule, and is by ISO 148-2 and ASTM E23, which are standards established by the Organization for Standardization. International set-up. The parameters of the machine are impact energy: 250 J / 500 J, impact speed: 5.24 m/s, pendulum front elevation angle: 150° and impact blade thickness: 16 mm.

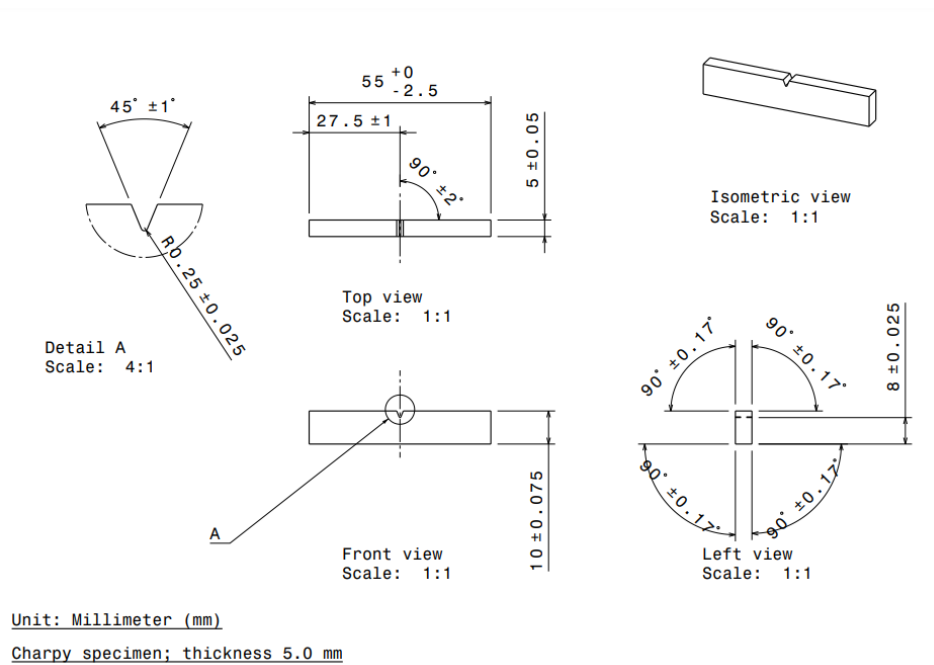


Figure 3.49 ASTM E2



Figure 3.50 Universal Pendulum Charpy Impact Tester, 500 Joule

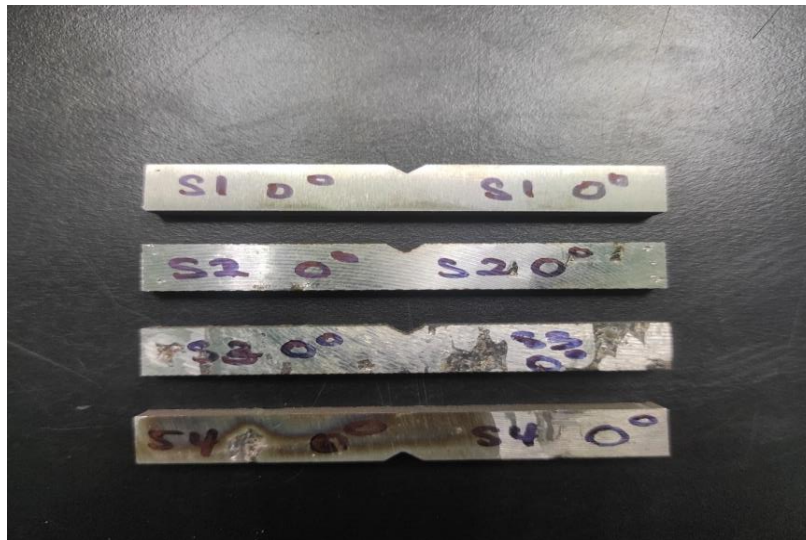


Figure 3.51 Specimen of 0° before impact test



Figure 3.52 Specimen of 0° after impact test

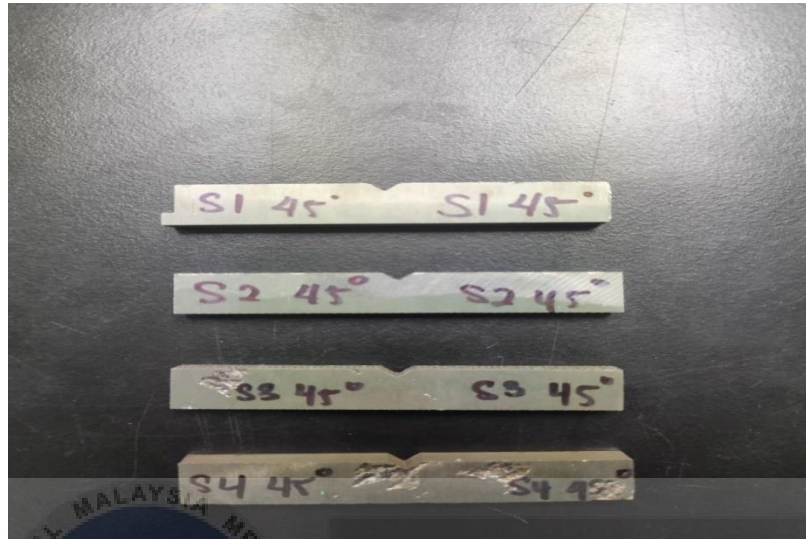


Figure 3.53 Specimen of 45° before impact test

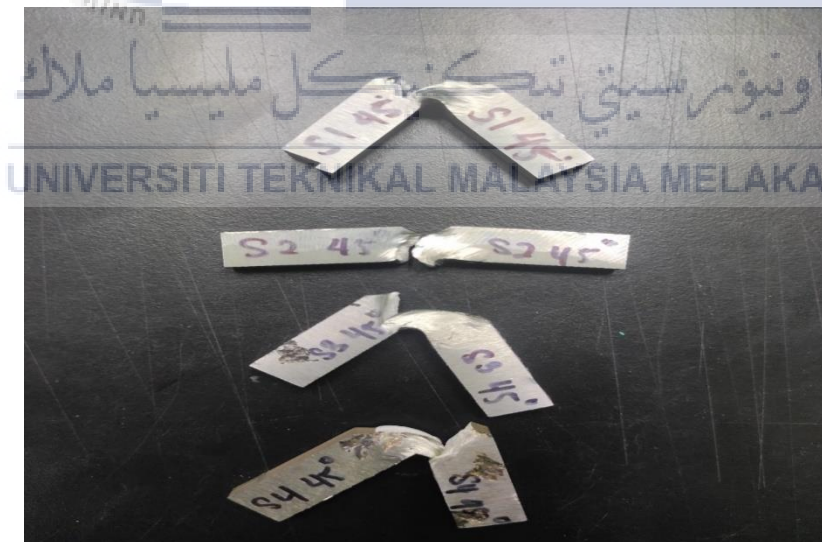


Figure 3.54 Specimen of 45° after impact test

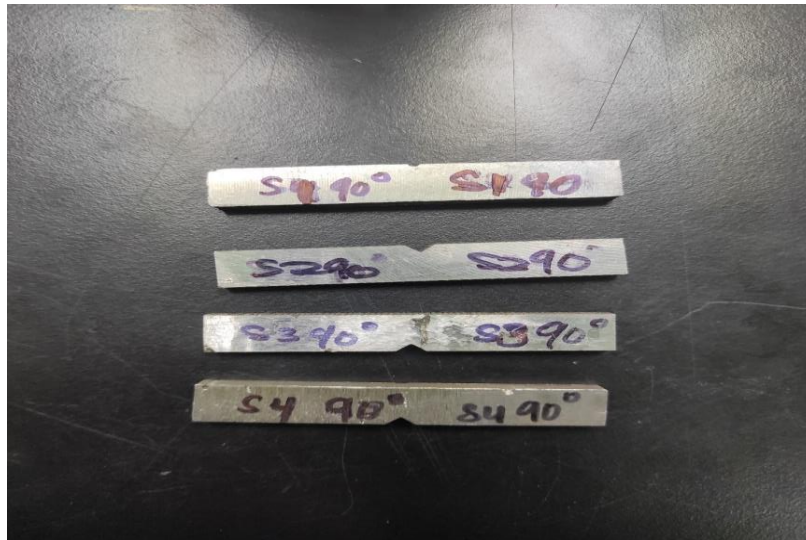


Figure 3.55 Specimen of 90° before impact test



Figure 3.56 Specimen of 90° after impact test

3.8.3 Hardness Test

Conducting hardness tests in WAAM is important to assess the mechanical properties of the fabricated parts and ensure they meet the required specifications. The hardness test helps determine the material's resistance to indentation or scratching, which provides insights into its strength, durability, and suitability for specific applications. This test follows ASTM E 92. The samples were cut at 90° aligned to build direction. Tests were conducted using the Vicker Microhardness Test, the parameter for the machine was the type of indenter Vickers, the load was 19.61 N and the hold time was 10 s. The tests were performed at various zones such as bottom, center, and top. The tests were conducted five times for the top zone, centre zone and bottom zone. The results from every zone will be calculated to average and the data will be plotted into a graph.



Figure 3.57 Vickers Hardness Tester. Shimadzu HMV-G31.

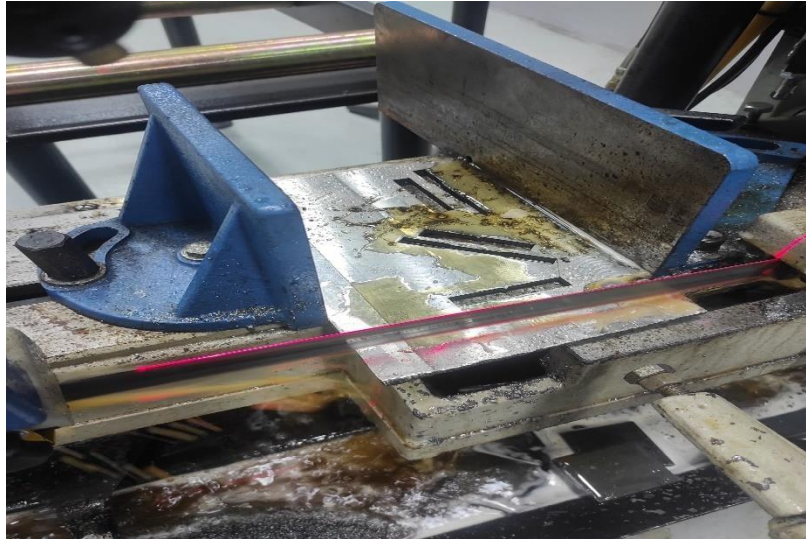


Figure 3.58 Cutting Sample Hardness from sample



Figure 3.59 Sample after the cutting process



Figure 3.60 Sample for Hardness Test



Figure 3.61 sample tested

3.9 Microstructural Analysis

The microstructure of a part created by WAAM is influenced by many different factors, including welding parameters, such as arc current, voltage, travel speed, and wire feed speed, as well as the properties and composition of the material. Because it directly influences the mechanical characteristics and functionality of the finished manufactured part, microstructure is crucial to comprehend and manage.

3.9.1 Optical Microscope

An optical microscope is a kind of microscope that enlarges images of small objects using a lens system and visible light. The most common and ancient kinds of microscopes are light ones. Numerous disciplines, such as biology, medicine, materials science, and electronics, use them.

Optical microscopes can be used to magnify objects by up to 2,000 times, which is enough to see individual cells and other microscopic structures. Optical microscopes are often used in combination with other techniques, such as staining and fluorescence microscopy, to enhance the contrast and visibility of specimens.

The samples were cut at 90° aligned to build direction as shown in Figure 3.63. Hot mounting presses were then used to encapsulate the specimens for us to hold the specimens

for etching, polishing, and grinding. Sandpaper grits of 180, 240, 300, 400, 600, 800, 1000, and 1200 were used to grind the specimens for approximately ten minutes until there were no visible scratches. Following that, the specimens were polished for approximately ten minutes using Diamant polycrystalline diamond and polish cloth (1μ and 3μ) to perform mirror surface. After that, the specimens will be etched for two minutes using the solution V2A etchant. The specimens will then be cleaned, dried with a hand blower, and placed under an optical microscope. After performing the microstructure analysis, the outcome was noted.



Figure 3.62 Optical Microscope ZEISS AxioCam ERc 5s

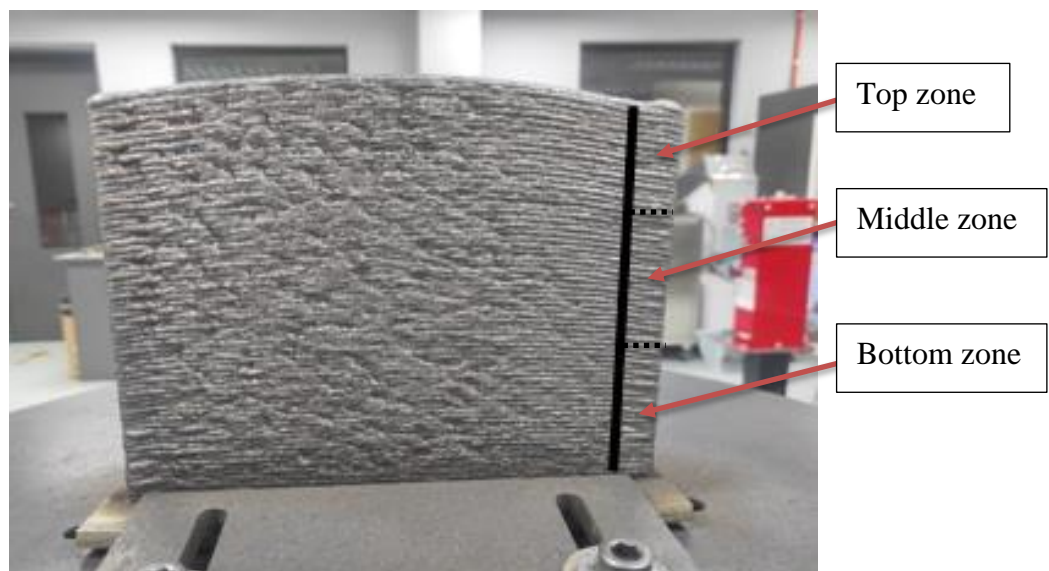


Figure 3.63 Microstructure sample (90° aligned to build direction)



Figure 3.64 Cutting samples.



Figure 3.65 Mounting press machine Ecorpes 100

Table 3.5 Parameter for hot mounting press

Heating temp (°C)	Pressure (atm)	Heating time (minute)	Mould size (mm)	Cool temperature (°C)	Type of powder
180	200	4	25	35	Phenolic powder



Figure 3.66 The specimens were encapsulated by using hot mounting presses. From left bottom, centre and top.

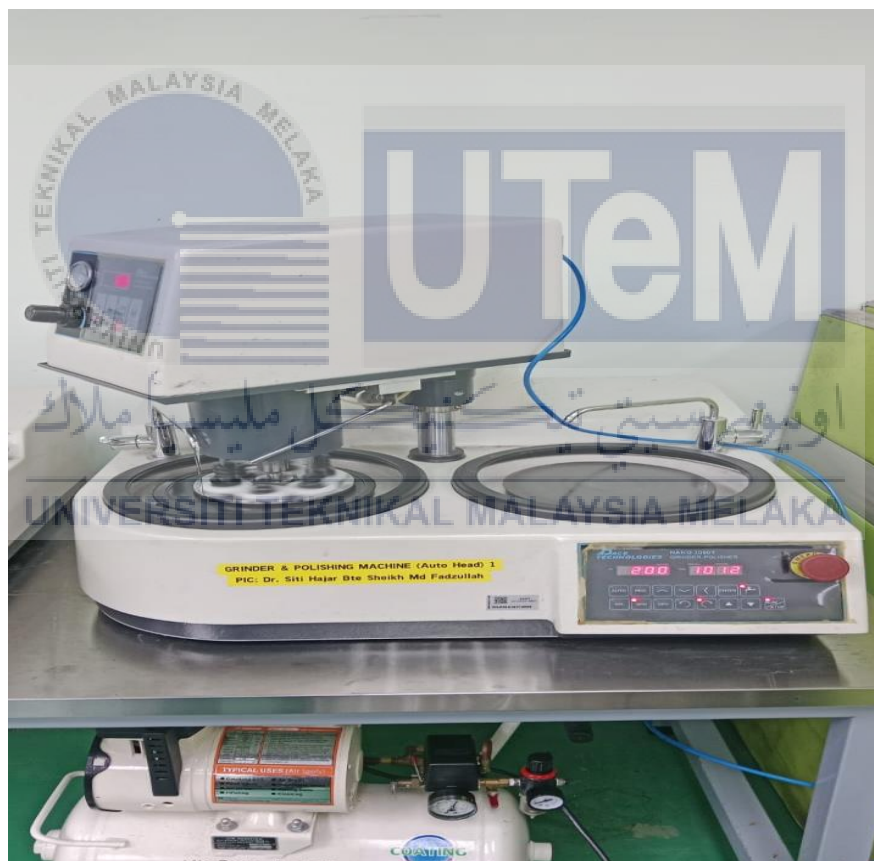


Figure 3.67 Grind process



Figure 3.68 Polish process



Figure 3.69 Etching process



Figure 3.70 Microstructure analysis

CHAPTER 4

RESULTS AND DISCUSSION

4.1 Introduction

The research on the mechanical characteristics and microstructure of stainless steel 308LSI arc wire will be covered in this chapter. First, the findings of the microstructure analysis and mechanical properties of the structures will be shown. Data from a literature review can be incorporated into this chapter to improve the reasoning behind each result for both analyses.

4.2 Results and Analysis of Mechanical Properties and Microstructural Analysis

An analysis of 308L steel walls produced by Wire Arc Additive Manufacturing (WAAM) provides important information about the mechanical and microstructural characteristics of the samples.

4.2.1 Tensile Test

The purpose of using a tensile test is to assess and evaluate the mechanical properties of the specimen, specifically their tensile strength, yield strength, and elongation. The tensile specimen measuring cuts of dimension 75 mm x 7.5 mm x 3.3 mm. The dog bone tensile specimen is processed and cut using an EDM wire cut machine to generate the specimen with the needed and precise dimensions.

In terms of mechanics, a material is said to have strength if it can withstand an applied force or stress without failing or deforming plastically. The material behaviour of a material is determined via the construction of a stress-strain curve. The curve made it possible to locate the fracture point, yield, and necking. Between elastic behaviour and the start of plastic deformation is the yield point. The point at which the material fails is what separates the necking point from the fracture point.

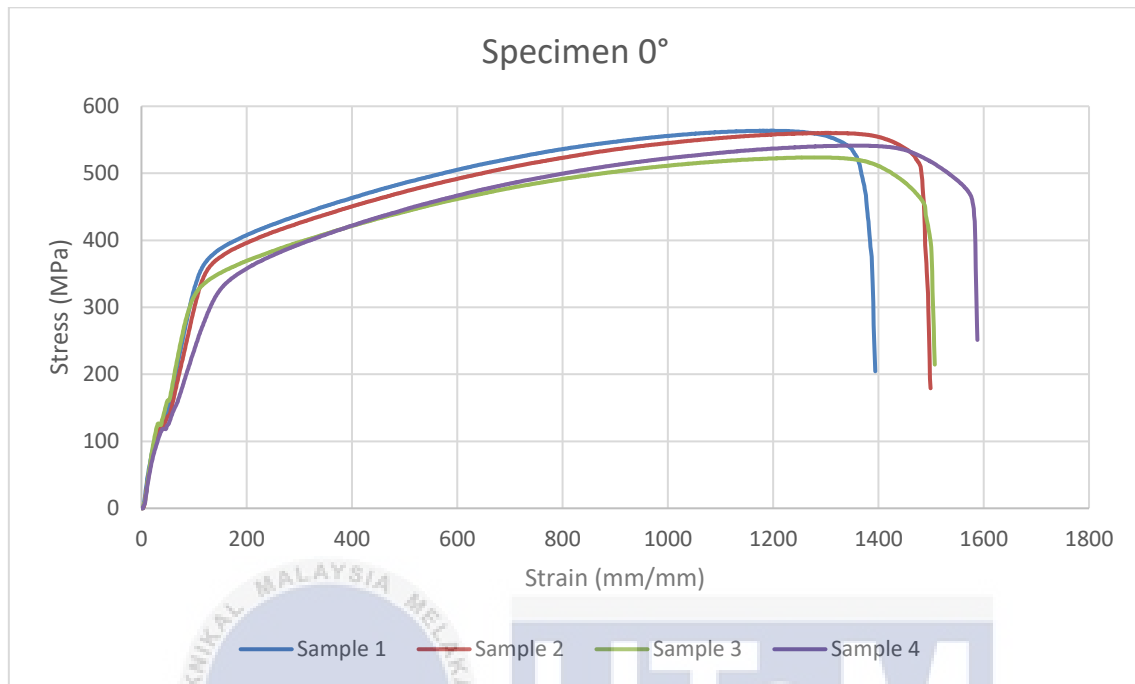


Figure 4.1 Graph for specimen 0°

Table 4.1 Tensile test result for specimen 0°

Sample	Young's Modulus (MPa)	Maximum Load (kN)	Tensile stress at Maximum Load (MPa)	Tensile strain (Extension) at Maximum Load (mm/mm)
1	16784.170	8.368	563.529	0.329
2	15703.463	8.319	560.182	0.361
3	19169.321	7.777	523.693	0.354
4	13631.929	8.039	541.331	0.373
Average	16322.221	8.126	547.183	0.354

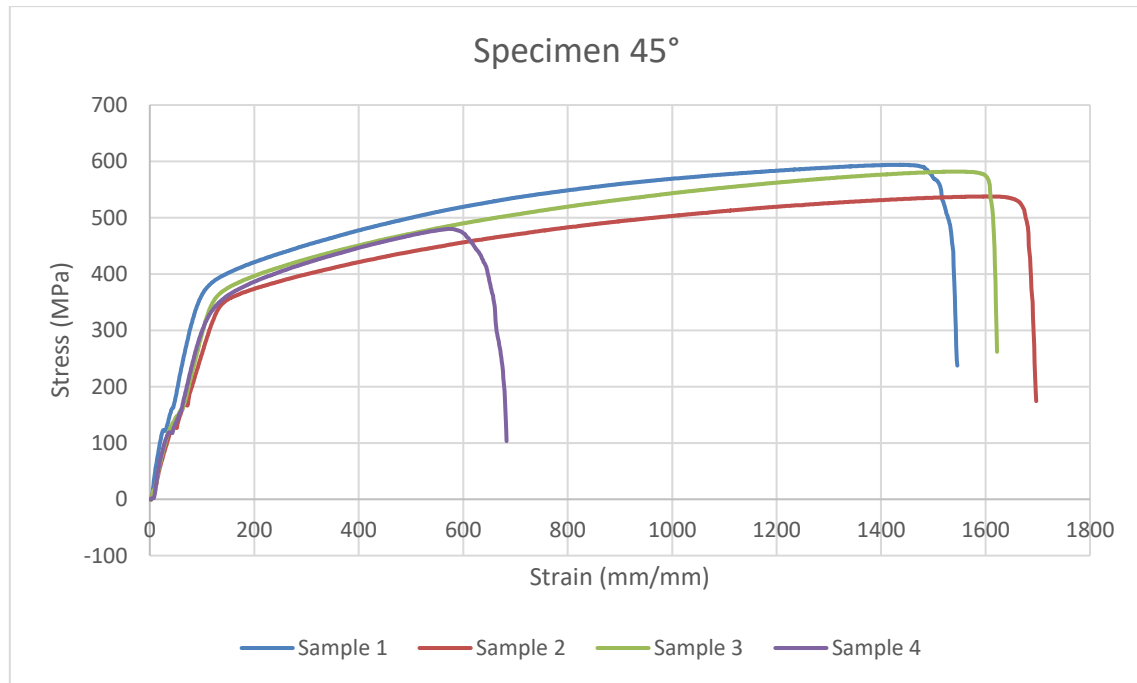


Figure 4.2 Graph for specimen 45°

Table 4.2 Tensile test result for specimen 45°

Sample	Young's Modulus (MPa)	Maximum Load (kN)	Tensile stress at Maximum Load (MPa)	Tensile strain (Extension) at Maximum Load (mm/mm)
1	21622.018	8.822	594.086	0.400
2	12831.234	7.986	537.801	0.445
3	14552.662	8.641	581.858	0.429
4	17225.906	7.128	479.990	0.159
Average	16557.955	8.144	548.434	0.358

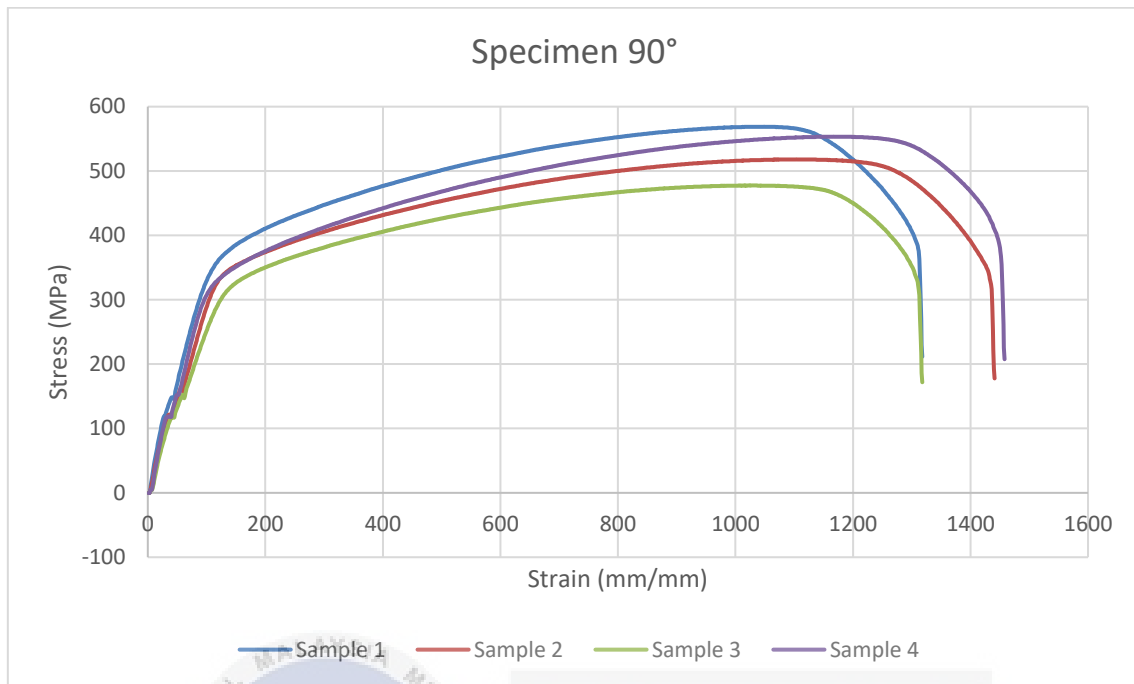


Figure 4.3 Graph for specimen 90°

Table 4.3 Tensile test result for specimen 90°

Sample	Young's Modulus (MPa)	Maximum Load (kN)	Tensile stress at Maximum Load (MPa)	Tensile strain (Extension) at Maximum Load (mm/mm)
1	17097.526	8.447	568.841	0.291
2	14720.178	7.694	518.098	0.306
3	13405.937	7.091	477.542	0.284
4	17662.551	8.218	553.386	0.323
Average	15721.548	7.863	529.467	0.301

Table 4.4 Average Values of the tensile test at different specimen angles (0°, 45°, 90°).

	0°	45°	90°
Average	547.183 MPa	548.434 MPa	529.467 MPa
Standard deviation	18.459	51.636	40.612

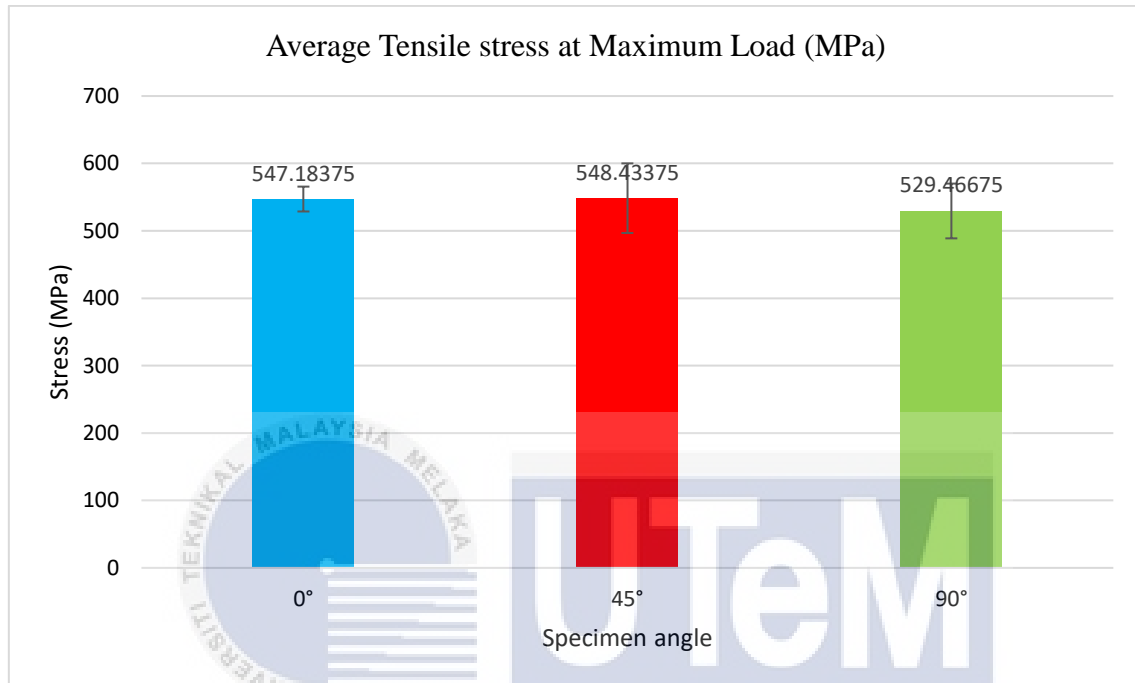


Figure 4.4 Graph for Tensile stress at Maximum Load (MPa) at different angles of specimens

The provided data represents the tensile properties of a material specimen at different angles. Comparing the three angles (0°, 45°, and 90°), the specimen at a 45° angle exhibits the highest Young's Modulus (16557.955 MPa), maximum load (8.144 kN), tensile stress at maximum load (548.434 MPa) and it achieves the highest tensile strain at maximum load (0.358 mm/mm) than specimen at 0° and 90°. This result aligned with (Laghi et al., 2020). This result is due to the upward growth of columnar dendrites.(Nagasai et al., 2022). The upward growth of columnar often leads to anisotropic mechanical properties. This is because the long, aligned grains can offer different levels of resistance to stress depending on their orientation relative to the applied load.

4.2.2 Impact Test

Four samples that have specimens at angles 0° , 45° and 90° have been tested for the Charpy impact test. This main purpose is to calculate the average value of the data, for each specimen with a dimension of 55 x 10 x 5 mm. The result is shown in Tables 4.4, 4.5, and 4.6. Impact testing is used to assess a material's impact toughness. This is the tenacity and ability of the material to absorb energy and withstand unforeseen loads

Table 4.5 Result of Charpy Impact Test for Specimen - 0°

Test Standard	ASTM E23	Batch No	Sample - 0°
Notch type	V	Notch Depth(mm)	2
Temperature	0	Operator	SAIFULLAIL
No.	Area	Impact Toughness	Absorbed Energy
	mm ²	J/cm ²	J
1	40	153.001	61.20
2	40	162.134	64.85
3	40	162.134	64.85
4	40	173.020	69.21
Average	40.000	162.572	65.03

Table 4.6 Result of Charpy Impact Test for Specimen - 45°

Test Standard	ASTM E23	Batch No	Sample - 45°
Notch type	V	Notch Depth(mm)	2
Temperature	0	Operator	SAIFULLAIL
No.	Area	Impact Toughness	Absorbed Energy
	mm ²	J/cm ²	J
1	40	183.493	73.40
2	40	158.359	63.34
3	40	165.384	66.12
4	40	173.215	70.09
Average	40.000	170.613	68.25

Table 4.7 Result of Charpy Impact Test for Specimen - 90°

Test Standard	ASTM E23	Batch No	Sample - 90°
Notch type	V	Notch Depth(mm)	2
Temperature	0	Operator	SAIFULLAIL
No.	Area	Impact Toughness	Absorbed Energy
	mm ²	J/cm ²	J
1	40	166.470	66.59
2	40	130.965	52.39
3	40	154.604	61.84
4	40	168.103	67.24
Average	40.000	155.036	62.01

Table 4.8 Data for Charpy Impact Test Energy Absorbed

	0°	45°	90°
Average	65.03 J	68.25 J	62.01 J
Standard deviation			

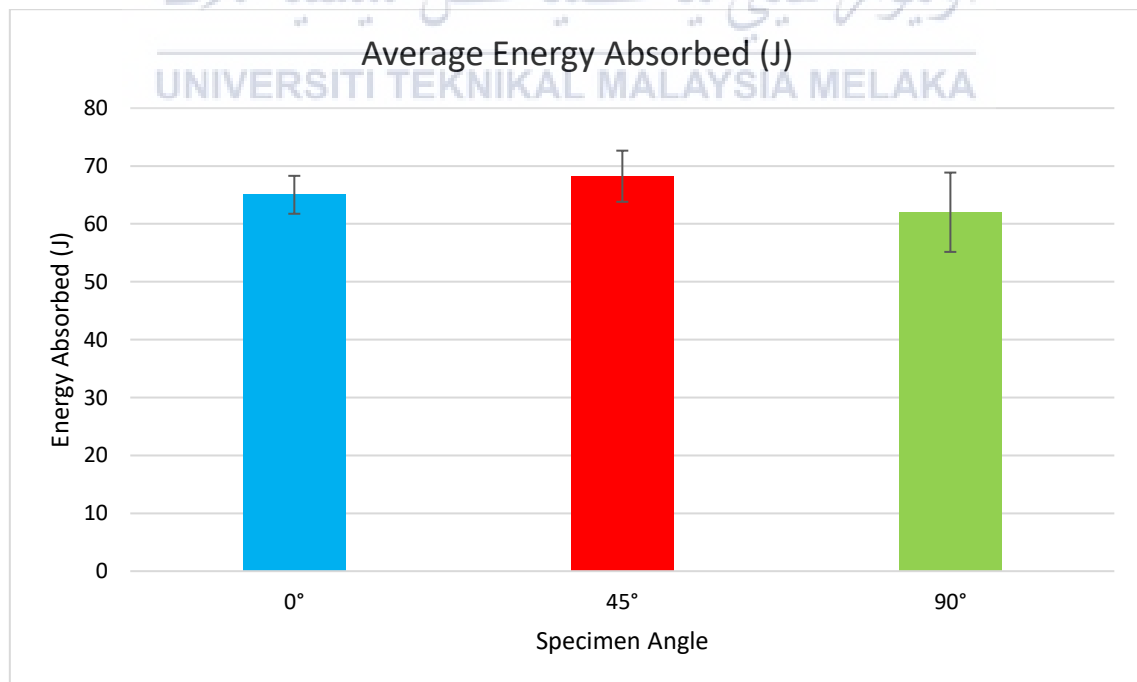


Figure 4.5 Graph of Average Energy Absorbed (J) at different angles of specimen

Energy absorbed was measured at three different angles (0° , 45° and 90°). Four samples were tested, and their average reading was taken for analysis. Figure 4.5 shows the graph for average energy absorbed reading. The average reading of energy absorbed of 65.03 J, 68.25 J and 62.01 J were recorded for 0° , 45° and 90° specimens, respectively. The average energy absorbed for 45° specimens was higher than for 0° and 90° specimens. The 45° specimens absorbed significantly more energy (68.25 J) compared to the 0° (65.03 J) and 90° (62.01 J) specimens. This indicates that the material's ability to resist impact is not uniform in all directions. The different energy absorption values at different angles strongly suggest that the material's microstructure is not the same in all orientations. This means the arrangement of grains, grain boundaries, and other microstructural features vary with direction, leading to different mechanical properties. The way a material absorbs and distributes energy during impact is heavily influenced by its microstructure. Grain boundaries, for example, can act as barriers to crack propagation, and certain grain orientations can be more resistant to deformation.

4.2.3 Hardness Test

The process of measuring a material's resistance to permanent deformation—such as indentation or scratching—by another, usually harder material is known as hardness testing. This characteristic shows the degree to which a material can withstand impacts, scratches, indents, and localized deformation. One important component of hardness is resistance to indentation, which is useful for determining how long a material will last and whether it is appropriate for a given use.

Table 4.9 Result Hardness Value for Bottom Zone

Trial	Hardness Value (Hv)
1	177.891
2	181.707
3	183.66
4	176.029
5	179.784
Average	179.814

Table 4.10 Result Hardness Value for the Middle Zone

Trial	Hardness value (Hv)
1	165.443
2	167.14
3	168.863
4	167.998
5	168.863
Average	167.661

Table 4.11 Result Hardness Value for Top Zone

Trial	Hardness value (Hv)
1	162.126
2	167.998
3	167.14
4	170.613
5	155.784
Average	164.732

Table 4.12 Result Average Hardness Value

	Bottom	Middle	Top
Average	179.814 Hv	167.661 Hv	164.732 Hv
Standard deviation	3.0166	1.431	5.872

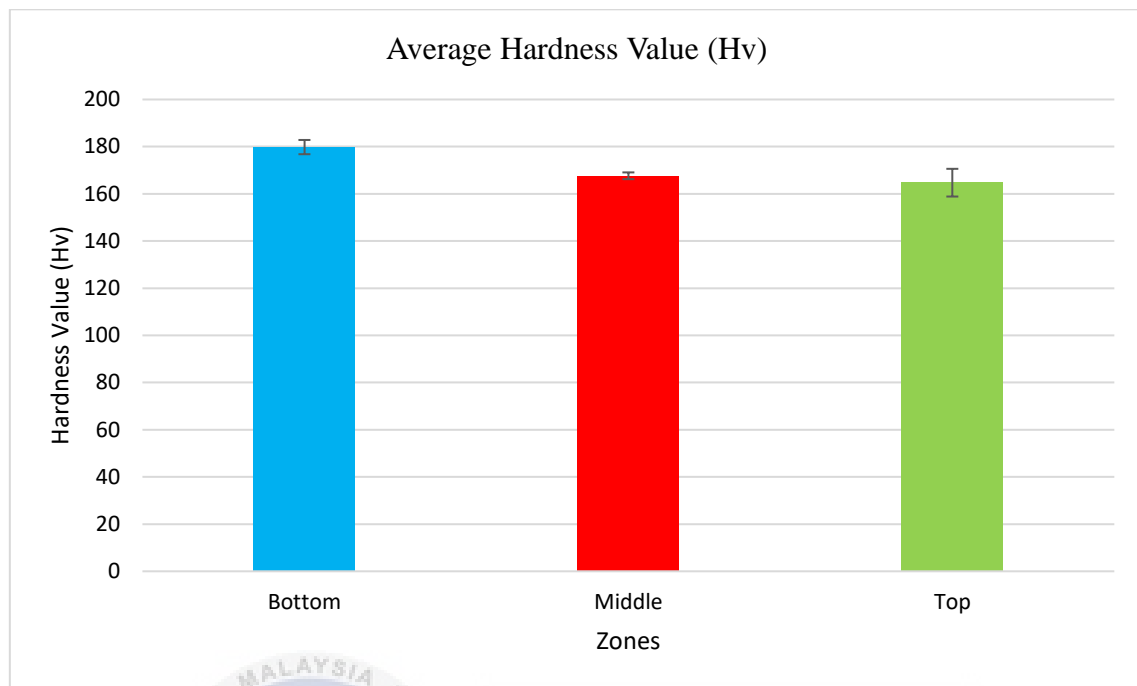


Figure 4.6 Graph for Average Hardness Value at different zones of specimens

The specimens were extracted from sample WAAM 308LSi 90° cross-section. The constructed multi-walled structure's bottom, middle, and top zones were measured for hardness. Five locations along the cross-section's centerline were used to measure each zone's hardness, and the average reading from these locations was recorded for analysis. Figure 4.6 displays the hardness reading graph. The bottom, centre, and top zones had average hardness readings of 179.814 Hv, 167.66 Hv, and 164.73 Hv, respectively. The bottom zone had a harder value than the top zone. This outcome was in line with (Le & Mai, 2020). The observed microstructures are consistent with the variation in microhardness. Based on Figure 4.6, the microstructure in this region is finer than in the other regions, which explains why the microhardness in the bottom zone has the highest average value.

4.2.4 Microstructural Analysis

The microstructure of the WAAM 308LSi 90° along the build direction of the sample was extracted from the cross-section between the bottom and top zones. The microstructure of specimens was observed in three zones: the bottom zone (Figure 4.7), the middle zone (Figure 4.8) and the top zone (Figure 4.9).

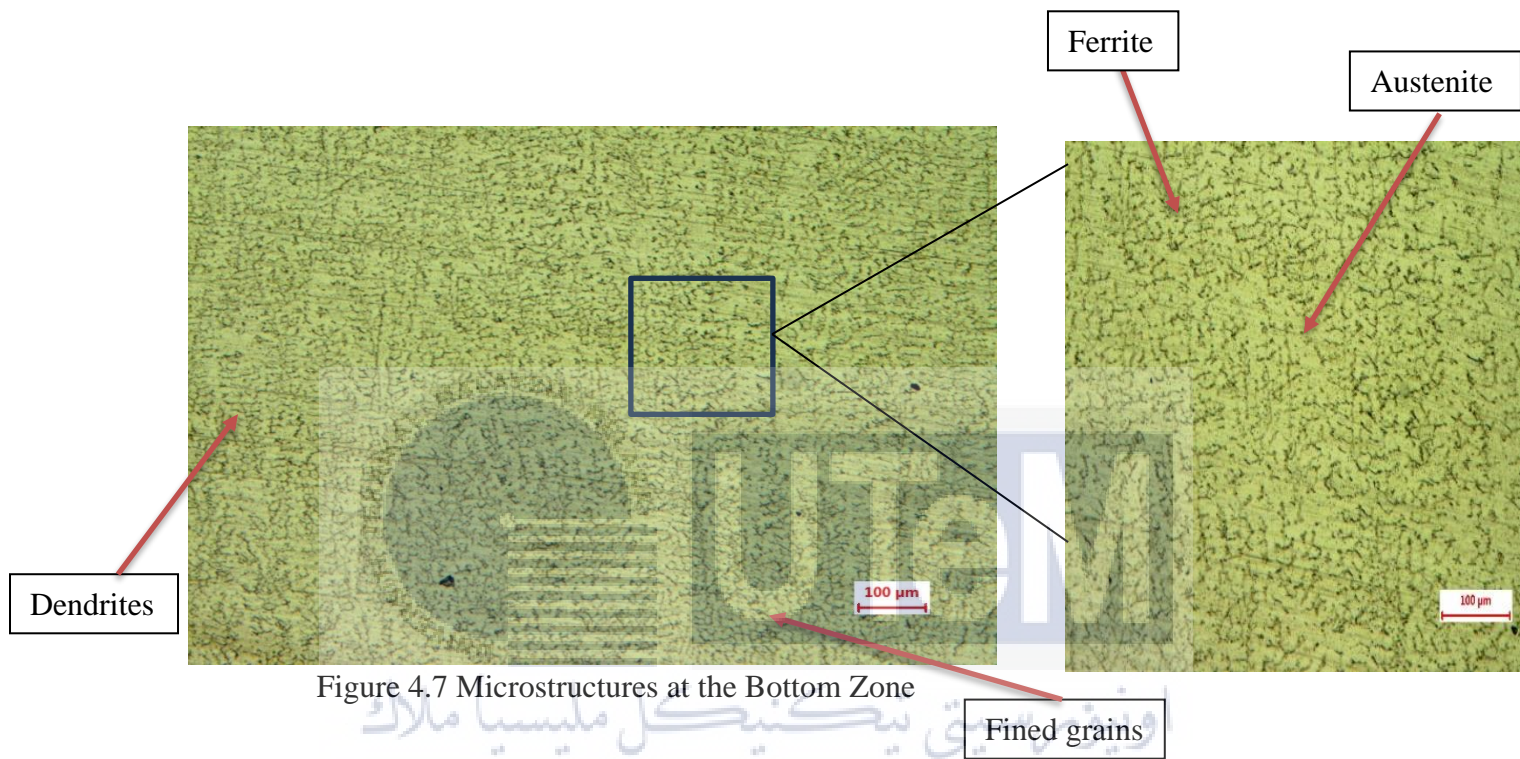


Figure 4.7 Microstructures at the Bottom Zone

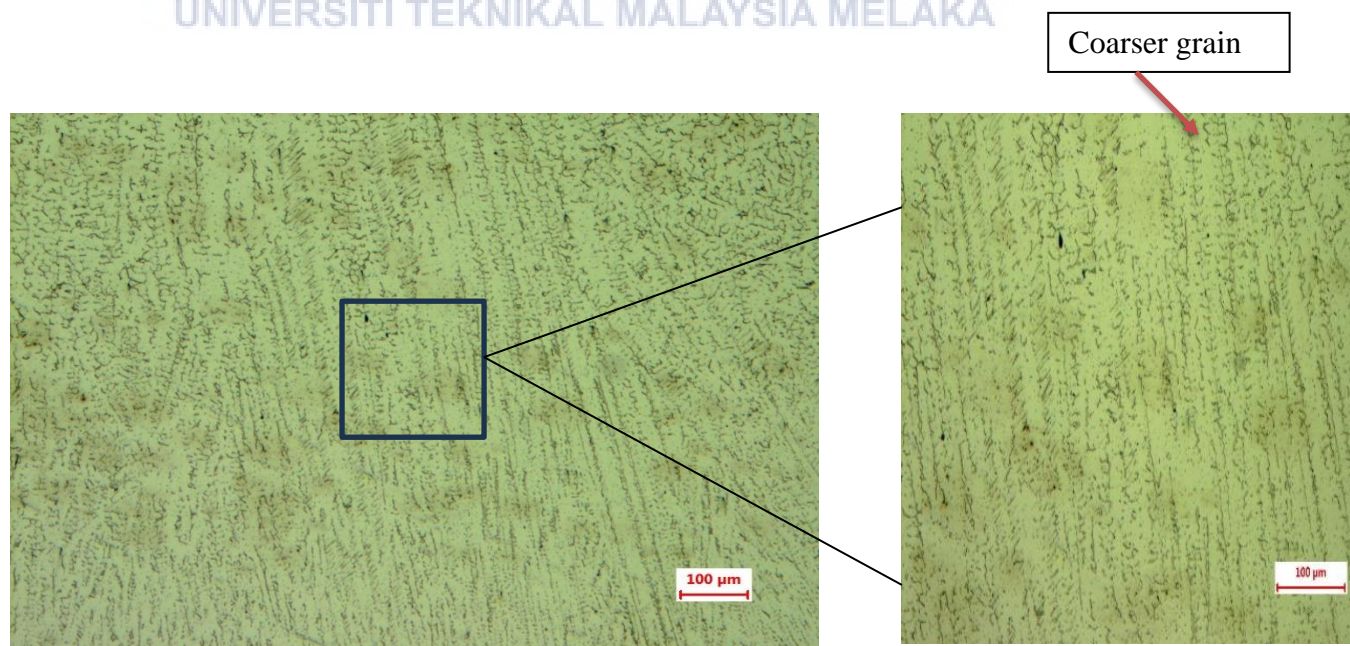


Figure 4.8 Microstructures at Middle Zone



Figure 4.9 Microstructure at Top Zone

The microstructure specimens were taken from the cross-section of sample CMT-WAAM 308LSi at 90° along with the build direction. The microstructure of specimens was observed in three zones: the bottom zone (Figure 4.7), the middle zone (Figure 4.8), and the top zone (Figure 4.9). The wall's microstructure is made up of austenite and ferrites. The build direction of the wall also affects the microstructure of the CMT-WAAM-walled 308LSi. Dendrites can be seen growing following the build direction in the bottom region as in (Figure 4.7). Because the heat is transferred directly to the substrate, leading to a higher cooling rate, the microstructures are also finer than in other zones. Finer grains, small size (having better strength and toughness), often formed during faster cooling processes or through specific treatments. The microstructure of the middle zone is coarser than that in the bottom zone (Figure 4.8) because when the deposition increase, heat accumulates, and the cooling rate is slower. Coarser grains, larger in size (better ductility), often formed during slower cooling processes. The top zone contacts directly with the air, and the time is also short, so it is composed of equiaxed grains (Figure 4.9). This result agrees with (Le & Mai, 2020).

4.3 Summary

Numerous studies have been conducted on the mechanical properties and microstructure of 308L stainless steel walls made using Wire Arc Additive Manufacturing (WAAM). Tensile tests revealed that specimens at 45° and 90° tend to have different mechanical properties. Specifically, specimens at 45° show the highest values for Young's Modulus, maximum load, and tensile stress at maximum load. The specimen at 45° displays the highest average energy absorption in the impact test, whereas the specimen at 90° displays lower average energy absorption values. In terms of average hardness, the bottom zone is harder than the top zone. The wall's build direction is reflected in variations in the microstructure of CMT-WAAM 308L. Dendrites growing following build directions are visible in the bottom region. Bottom zone show that the finer grain. Compared to the bottom zone, the middle zone's microstructure is coarser. The top zone is made up of equiaxed grains.



CHAPTER 5

CONCLUSION AND RECOMMENDATIONS

5.1 Conclusion

The current study examined the use of CMT-WAAM in the fabrication of 308LSi walls. The study's primary findings are summed up in terms of GMAW process variables, such as travel speed, voltage, and welding current, all of which have a big impact on the size and form of individual weld beads. Bead width is significantly influenced by voltage and travel speed, whereas bead height is significantly influenced by welding current and travel speed.

With the right processing parameters ($I = 115$ A, $U = 11.6$ V, and $v = 4.0$ m/min), we can create straightforward, regular, and smooth weld beads that have the right height and width. This guarantees the 308 LSi samples manufactured by CMT-WAAM are stable and of high quality. The CMT-WAAM 308L walls were built successfully and without any significant flaws, like cracks.

The mechanical properties and microstructural characteristics of 308L stainless steel walls produced through wire-arc additive manufacturing (WAAM) have been extensively studied. For mechanical properties, tensile tests show that the specimen at 45° exhibits the highest values for Young's Modulus, maximum load, and tensile stress at maximum load, while the specimen at 90° tends to have the lowest values for these properties. This result is the upward growth of columnar dendrites.

For the impact test, the specimen at 45° exhibits the highest average energy absorption, while the specimen at 90° has lower average energy absorption values. Microstructure variations may play a role, influencing its ability to absorb and distribute energy during impact and leading to anisotropic properties.

For the hardness test, the bottom zone has the highest average hardness compared to the top zone. The change in microhardness is consistent with the observation of microstructures. Based on Figure 4.6, the microstructure in this region is finer than in the other regions, which explains why the microhardness in the bottom zone has the highest average value. This means that the lower area is harder than the upper area.

The build direction of the wall affects the microstructure of the CMT-WAAM wall of 308LSi. Dendrites grow in following to build directions, and finer grains dominate in the bottom zone. Additionally, because heat is transferred directly to the substrate, leading to a higher cooling rate, the microstructures at the lower zone are finer than in other zones. Because heat builds up and cooling occurs more slowly as deposits get larger, the middle zone's microstructure is coarser than the bottom zone's. The top zone is made up of equiaxed grains because it has direct air contact and brief duration.

The thorough testing that was done, which included tensile, impact, and hardness tests among other mechanical tests, provided insightful information about the material's mechanical characteristics. Aspects like tensile strength, absorbed energy, and hardness value have all been investigated in these tests. A comprehensive understanding of the material's structure and qualities has also been obtained through a detailed analysis of its microstructural features.

5.2 Recommendations

For future improvements, the accuracy of the results could be enhanced as follows:

- a) Optimize processing parameters. Optimizing processing parameters in wire arc additive manufacturing is critical to achieving improved material properties and minimizing anisotropy.
- b) Conduct Research Study on Wall Structure: A research study should involve measuring the structure of walls before and after the milling process. This approach is essential to assess the impact on mechanical and microstructural properties.

- c) Implement Dwell Time between Layers: Adding dwell time after one layer to another is advised. This practice allows each layer to cool down before adding the next layer, potentially improving accuracy and minimizing thermal effects

5.3 Project Potential

The study findings offer a rich source of inspiration for researchers, providing a basis for exploring and advancing knowledge in the realm of mechanical properties. These insights can catalyze innovative projects aimed at improving construction materials and enhancing their performance.



REFERENCES

- Baoqiang, C., Ruijie, O., Bojin, Q., & Jialuo, D. (2016). *Influence of Cold Metal Transfer Process and Its Heat Input on Weld Bead Geometry and Porosity of Aluminum-Copper Alloy Welds*.
- Bikas, H., Stavropoulos, P., & Chrysosolouris, G. (2016). Additive manufacturing methods and modeling approaches: A critical review. *International Journal of Advanced Manufacturing Technology*, 83(1–4), 389–405. <https://doi.org/10.1007/s00170-015-7576-2>
- Dinovitzer, M., Chen, X., Laliberte, J., Huang, X., & Frei, H. (2019). Effect of wire and arc additive manufacturing (WAAM) process parameters on bead geometry and microstructure. *Additive Manufacturing*, 26, 138–146. <https://doi.org/10.1016/j.addma.2018.12.013>
- Evans, S. I., Xu, F., & Wang, J. (2023). Material properties and local stability of WAAM stainless steel equal angle sections. *Engineering Structures*, 287. <https://doi.org/10.1016/j.engstruct.2023.116160>
- Evjemo, L. D., Langelandsvik, G., Moe, S., Danielsen, M. H., & Gravdahl, J. T. (2022). Wire-arc additive manufacturing of structures with overhang: Experimental results depositing material onto fixed substrate. *CIRP Journal of Manufacturing Science and Technology*, 38, 186–203. <https://doi.org/10.1016/j.cirpj.2022.04.006>
- Haden, C. V., Zeng, G., Carter, F. M., Ruhl, C., Krick, B. A., & Harlow, D. G. (2017). Wire and arc additive manufactured steel: Tensile and wear properties. *Additive Manufacturing*, 16, 115–123. <https://doi.org/10.1016/j.addma.2017.05.010>
- Hadjipantelis, N., Weber, B., Buchanan, C., & Gardner, L. (2022). Description of anisotropic material response of wire and arc additively manufactured thin-walled stainless steel elements. *Thin-Walled Structures*, 171. <https://doi.org/10.1016/j.tws.2021.108634>
- Jin, W., Zhang, C., Jin, S., Tian, Y., Wellmann, D., & Liu, W. (2020). Wire arc additive manufacturing of stainless steels: A review. In *Applied Sciences (Switzerland)* (Vol. 10, Issue 5). MDPI AG. <https://doi.org/10.3390/app10051563>

- Laghi, V., Palermo, M., Tonelli, L., Gasparini, G., Ceschini, L., & Trombetti, T. (2020). Tensile properties and microstructural features of 304L austenitic stainless steel produced by wire-and-arc additive manufacturing. *International Journal of Advanced Manufacturing Technology*, 106(9–10), 3693–3705. <https://doi.org/10.1007/s00170-019-04868-8>
- Le, V. T., & Mai, D. S. (2020). Microstructural and mechanical characteristics of 308L stainless steel manufactured by gas metal arc welding-based additive manufacturing. *Materials Letters*, 271. <https://doi.org/10.1016/j.matlet.2020.127791>
- Le, V. T., Mai, D. S., Doan, T. K., & Paris, H. (2021). Wire and arc additive manufacturing of 308L stainless steel components: Optimization of processing parameters and material properties. *Engineering Science and Technology, an International Journal*, 24(4), 1015–1026. <https://doi.org/10.1016/j.jestch.2021.01.009>
- Li, J. L. Z., Alkahari, M. R., Rosli, N. A. B., Hasan, R., Sudin, M. N., & Ramli, F. R. (2019). Review of wire arc additive manufacturing for 3d metal printing. *International Journal of Automation Technology*, 13(3), 346–353. <https://doi.org/10.20965/ijat.2019.p0346>
- Nagasai, B. P., Malarvizhi, S., & Balasubramanian, V. (2022). Mechanical properties and microstructural characteristics of wire arc additive manufactured 308 L stainless steel cylindrical components made by gas metal arc and cold metal transfer arc welding processes. *Journal of Materials Processing Technology*, 307. <https://doi.org/10.1016/j.jmatprotec.2022.117655>
- Pan, Z., Ding, D., Wu, B., Cuiuri, D., Li, H., & Norrish, J. (2018). Arc Welding Processes for Additive Manufacturing: A Review. In *Transactions on Intelligent Welding Manufacturing* (pp. 3–24). Springer. https://doi.org/10.1007/978-981-10-5355-9_1
- Pérez, M., Carou, D., Rubio, E. M., & Teti, R. (2020). Current advances in additive manufacturing. *Procedia CIRP*, 88, 439–444. <https://doi.org/10.1016/j.procir.2020.05.076>
- Ryalat, M., ElMoaqet, H., & AlFaouri, M. (2023). Design of a Smart Factory Based on Cyber-Physical Systems and Internet of Things towards Industry 4.0. *Applied Sciences (Switzerland)*, 13(4). <https://doi.org/10.3390/app13042156>
- Selvi, S., Vishvakshnan, A., & Rajasekar, E. (2018). Cold metal transfer (CMT) technology - An overview. In *Defence Technology* (Vol. 14, Issue 1, pp. 28–44). China Ordnance Society. <https://doi.org/10.1016/j.dt.2017.08.002>

- Senthil, T. S., Babu, S. R., Puviyarasan, M., & Balachandar, V. S. (2023). Experimental investigations on the multi-layered SS316L wall fabricated by CMT-based WAAM: Mechanical and microstructural studies. *Journal of Alloys and Metallurgical Systems*, 2, 100013. <https://doi.org/10.1016/j.jalmes.2023.100013>
- Singh, S. R., & Khanna, P. (2021). Wire arc additive manufacturing (WAAM): A new process to shape engineering materials. *Materials Today: Proceedings*, 44, 118–128. <https://doi.org/10.1016/j.matpr.2020.08.030>
- Singh, S., Sharma, S. K., & Rathod, D. W. (2020). A review on process planning strategies and challenges of WAAM. *Materials Today: Proceedings*, 47, 6564–6575. <https://doi.org/10.1016/j.matpr.2021.02.632>
- Vora, J., Parmar, H., Chaudhari, R., Khanna, S., Doshi, M., & Patel, V. (2022). Experimental investigations on mechanical properties of multi-layered structure fabricated by GMAW-based WAAM of SS316L. *Journal of Materials Research and Technology*, 20, 2748–2757. <https://doi.org/10.1016/j.jmrt.2022.08.074>
- Wang, C., Zhu, P., Wang, F., Lu, Y. H., & Shoji, T. (2022). Anisotropy of microstructure and corrosion resistance of 316L stainless steel fabricated by wire and arc additive manufacturing. *Corrosion Science*, 206. <https://doi.org/10.1016/j.corsci.2022.110549>
- Wang, L., Xue, J., & Wang, Q. (2019). Correlation between arc mode, microstructure, and mechanical properties during wire arc additive manufacturing of 316L stainless steel. *Materials Science and Engineering A*, 751, 183–190. <https://doi.org/10.1016/j.msea.2019.02.078>
- Wu, B., Pan, Z., Ding, D., Cuiuri, D., Li, H., Xu, J., & Norrish, J. (2018). A review of the wire arc additive manufacturing of metals: properties, defects and quality improvement. In *Journal of Manufacturing Processes* (Vol. 35, pp. 127–139). Elsevier Ltd. <https://doi.org/10.1016/j.jmapro.2018.08.001>
- Xia, C., Pan, Z., Polden, J., Li, H., Xu, Y., Chen, S., & Zhang, Y. (2020). A review on wire arc additive manufacturing: Monitoring, control and a framework of automated system. In *Journal of Manufacturing Systems* (Vol. 57, pp. 31–45). Elsevier B.V. <https://doi.org/10.1016/j.jmsy.2020.08.008>

APPENDICES

APPENDIX A Gant Chart PSM 1

Activities	Status	Week													
		1	2	3	4	5	6	7	8	9	10	11	12	13	14
Title registration with supervisor	Plan														
	Actual														
Project explanation from the supervisor	Plan														
	Actual														
Drafting & writing Chapter 1	Plan														
	Actual														
Correction for Chapter 1	Plan														
	Actual														
Drafting & writing Chapter 2	Plan														
	Actual														
Correction for Chapter 2	Plan														
	Actual														
Drafting & writing Chapter 3	Plan														
	Actual														
Correction for Chapter 3	Plan														
	Actual														
Submit draft report (chapter 1,2,3) to supervisor to check it.	Plan														
	Actual														
Finalize report PSM 1 before submission	Plan														
	Actual														

APPENDIX B Gant Chart PSM 2

Activities	Status	Week													
		1	2	3	4	5	6	7	8	9	10	11	12	13	14
PSM 2 implementation	Plan														
	Actual														
Discussion with supervisor	Plan														
	Actual														
Method used for the experiment	Plan														
	Actual														
Experiment setup	Plan														
	Actual														
Material and equipment selection and supervisor meeting	Plan														
	Actual														
Experiments and testing	Plan														
	Actual														
Listing all results	Plan														
	Actual														
Writing chapter 4	Plan														
	Actual														
Writing chapter 5	Plan														
	Actual														
The report checked by the supervisor	Plan														
	Actual														